Nonlinear Silicon Photonics: Analytical Tools

Ivan D. Rukhlenko, Malin Premaratne, *Senior Member, IEEE*,
and Govind P. Agrawal, *Fellow, IEEE*

(Invited Paper)

***Abstract*—Since the recent demonstration of chip-scale, silicon-based, photonic devices, silicon photonics provides a viable and promising platform for modern nonlinear optics. The development and improvement of such devices are helped considerably by theoretical predictions based on the solution of the underlying nonlinear propagation equations. In this paper, we review the approximate analytical tools that have been developed for analyzing active and passive silicon waveguides. These analytical tools provide the much needed physical insight that is often lost during numerical simulations. Our starting point is the coupled-amplitude equations that govern the nonlinear dynamics of two optical waves interacting inside a silicon-on-insulator waveguide. In their most general form, these equations take into account not only linear losses, dispersion, and the free-carrier and Raman effects, but also allow for the tapering of the waveguide. Employing approximations based on physical insights, we simplify the equations in a number of situations of practical interest and outline techniques that can be used to examine the influence of intricate nonlinear phenomena as light propagates through a silicon waveguide. In particular, propagation of single pulse through a waveguide of constant cross section is described with a perturbation approach. The process of Raman amplification is analyzed using both purely analytical and semianalytical methods. The former avoids the undepleted-pump approximation and provides approximate expressions that can be used to discuss intensity noise transfer from the pump to the signal in silicon Raman amplifiers. The latter utilizes a variational formalism that leads to a system of nonlinear equations that governs the evolution of signal parameters under the continuous-wave pumping. It can also be used to find an optimum tapering profile of a silicon Raman amplifier that provides the highest net gain for a given pump power.**

***Index Terms*—Free-carrier absorption (FCA), integrated optics, Kerr effect, nonlinear optics, optical pulse propagation, Raman effect, silicon photonics, silicon Raman amplifiers, silicon waveguides, two-photon absorption (TPA), waveguide tapering.**

I. Introduction

THE problem of light propagation through silicon waveguides with characteristic lateral dimensions of the order of 1 μm has been extensively studied in recent years, both experimentally [1]–[11] and theoretically [12]–[22], because of its immense practical applications [23]–[27]. The main reason why silicon is considered a promising photonics material stems from its relatively strong nonlinear interaction with external electromagnetic fields whose wavelengths lie in the transparent infrared region beyond 1.1 μm. Since this region includes the telecommunication window near 1.55 μm, a multitude of nonlinear optical effects inside silicon waveguides can be used for diverse beneficial applications. Moreover, these nonlinear interactions can be further enhanced by employing silicon-on-insulator (SOI) waveguides in which a tight-mode confinement provides large optical intensities even at moderate input power levels. Therefore, it is not surprising that, to date, almost all physical properties of silicon have found applications in different nonlinear SOI-based photonic devices [26], [28]–[30]. For example, stimulated Raman scattering (SRS), which is particularly strong in silicon [31]–[33], is employed to make optical amplifiers [34]–[42], modulators [43], and Raman lasers [44]–[52]. The Kerr effect is successfully applied for optical phase modulation [53], [54], soliton formation [6], and supercontinuum generation [29], [55]–[57]. The phenomenon of four-wave mixing by itself, or in combination with SRS, has been used to make broadband frequency converters [58]–[66]. Although two-photon absorption (TPA) by itself is undesirable, it has been demonstrated that TPA-induced free-carrier generation and thermooptic effects are suitable for all-optical switching [67]–[71], modulation [72], and pulse compression [73], [74]; they can also be used for autocorrelation measurements [75], [76]. The natural compatibility of SOI technology with the existing silicon manufacturing process opens up wide possibilities for utilizing these and other useful functionalities in fabricating photonic integrated circuits.

To date, nonlinear propagation of optical pulses through silicon waveguides has been studied mostly numerically by using the well-known, split-step Fourier method [77]. It makes use of the widely deployed slowly varying envelope approximation to separate a rapidly varying waveform (the carrier) from the signal (the envelope) [12], [13], [77]. Another numerical method, which is often used for a direct solution of the Maxwell's equations, is the finite-difference time-domain (FDTD) method [78]–[80]. Since it does not make use of the slowly varying envelope approximation, the FDTD scheme is well suited for studying the propagation of pulses as short as a single optical cycle. In principle, these two numerical methods can provide comprehensive information and model all types of nonlinear phenomena inside silicon waveguides. In spite of this, simple analytical solutions and semianalytical tools are of considerable value in practice because they offer a clearer view of nonlinear processes in silicon waveguides and

Manuscript received April 3, 2009; revised June 2, 2009. First published September 22, 2009; current version published February 5, 2010. This work was supported by the Australian Research Council through its Discovery Grant Scheme under Grant DP0877232. The work of G. P. Agrawal was supported by the National Science Foundation (NFS) Award ECCS-0801772.

I. D. Rukhlenko and M. Premaratne are with the Advanced Computing and Simulation Laboratory (AχL), Department of Electrical and Computer Systems Engineering, Monash University, Clayton, Vic. 3800, Australia (e-mail: ivan.rukhlenko@eng.monash.edu.au; malin@eng.monash.edu.au).

G. P. Agrawal is with the Institute of Optics, University of Rochester, Rochester, NY 14627-0186 USA (e-mail: gpa@optics.rochester.edu).

Digital Object Identifier 10.1109/JSTQE.2009.2026435

may open up nontrivial paths for device optimization. Over the past few years, a number of such methods have been proposed in literature on nonlinear silicon photonics. In this paper, we outline the basic ideas that underlie these methods and review the results with the purpose of stimulating further progress in this direction.

This review is organized as follows. In Section II, we briefly discuss the origin of the well-known coupled-amplitude equations that describe nonlinear interaction between two waves of different carrier frequencies. These equations are written in their most general form and include not only the dispersive, free-carrier, and Raman effects, but also changes in the effective mode area (EMA) along a tapered silicon waveguide. In the case of a single wave launched into the waveguide such that SRS does not occur, a single integro-differential equation is sufficient to describe the nonlinear nature of wave propagation. An approximate analytical solution of this equation is presented in Section III. In Section IV, we discuss an approximate analytical solution for a continuous-wave (CW) Raman amplifier with constant lateral cross section. This solution avoids the undepleted-pump approximation and leads to the generalized definition of the effective length with regard to nonlinear absorption. We use this solution to analyze the peculiarities of relative intensity noise (RIN) transfer in silicon Raman amplifiers. Sections V and VI are devoted to semi-analytical methods that show the usefulness of the variational approach for tackling complicated nonlinear problems. In Section V, we describe a method for analyzing the dynamics of pulse parameters under CW-pumped Raman amplification. Section VI focuses on the variational problem of gain optimization by appropriate waveguide tapering. First, we consider the undepleted-pump approximation that admits analytical solution. After that, we recast it as a boundary-value problem that is solved to obtain the optimal waveguide profile that maximizes the net gain of the amplifier for a given pump power. We summarize our study in Section VII and conclude the review.

II. Generalized Propagation Equations for Active Silicon Waveguides

Let us consider the nonlinear interaction of two optical waves of different carrier wavelengths (called the pump and the signal) inside a silicon crystal waveguide. To make the applicability domain of the following analysis as wide as possible, we consider a silicon waveguide whose cross-section area may vary along its length because of tapering of its width. During their propagation, the two optical fields induce material polarization $\mathbf{P}(\mathbf{r},t)$. This polarization drives the evolution of total electric field $\mathbf{E}(\mathbf{r},t)$ according to the Maxwell wave equation [77], [81]

$$\nabla^2\mathbf{E}-\frac{1}{c^2}\frac{\partial^2\mathbf{E}}{\partial t^2}=\frac{1}{\varepsilon_0 c^2}\frac{\partial^2\mathbf{P}}{\partial t^2} \tag{1}$$

where ε_0 is the free-space permittivity and c is the speed of light in vacuum.

The polarization of silicon can be represented as a sum of linear and nonlinear parts $\mathbf{P}(\mathbf{r},t)=\mathbf{P}_{\rm L}(\mathbf{r},t)+\mathbf{P}_{\rm NL}(\mathbf{r},t)$. The nonlinear contribution originates from SRS, polarization of bound electrons, and refractive index changes induced by the photogenerated free carriers [12]. These effects complicate substantially not only theoretical but even numerical investigation of nonlinear interactions governed by (1). To simplify the analysis, several physically reasonable assumptions need to be introduced. First, we assume that both incident waves are linearly polarized such that they excite either the fundamental TE or the TM mode of the waveguide. We also suppose that the nonlinear part of polarization does not affect the lateral mode profiles associated with the pump and signal waves $F_p(\mathbf{r})$ and $F_s(\mathbf{r})$, but it influences their z-dependent envelopes $A_p(z,t)$ and $A_s(z,t)$. At the same time, the dependence of mode profiles on propagation distance z, caused by the nonuniform cross section of the waveguide, is assumed to be much weaker than the corresponding dependence of envelopes. Finally, we assume that both optical waves propagate only in the forward, $+z$, direction. It amounts to assuming that any reflections are so weak that backward propagating waves can be safely discarded. This assumption, together with the slowly varying envelope approximation, allows one to reduce the order of z derivative in (1) from 2 to 1.

To proceed further, we write the total electric field at a point $\mathbf{r}=(x,y,z)$ inside silicon waveguide in the following form:

$$E(\mathbf{r},t)=s_p(z)F_p(\mathbf{r})A_p(z,t)\exp[i(\beta_{0p}z-\omega_p t)] +s_s(z)F_s(\mathbf{r})A_s(z,t)\exp[i(\beta_{0s}z-\omega_s t)]+\text{c.c.}$$

where $\omega_u=2\pi c/\lambda_u$ ($u=p$ or s for the pump and signal waves, respectively) is the carrier frequency, $\beta_{0u}=n_{0u}k_u$ is the propagation constant, $k_u=\omega_u/c$ is the free-space wavenumber, and n_{0u} is the effective refractive index. To account for the waveguide tapering, we have also introduced $s_u(z)$ as the shape function.

By means of a standard procedure (see, e.g. [12] or [13]), the wave equation (1) can be reduced to the system of the following two coupled-amplitude equations that govern the evolution of the pump and signal envelopes inside the SOI waveguide:

$$\begin{aligned}\frac{\partial A_p}{\partial z}&+\beta_{1p}\frac{\partial A_p}{\partial t}+\frac{i\beta_{2p}}{2}\frac{\partial^2 A_p}{\partial t^2}=-\frac{\alpha_p}{2}A_p\\&+i(\gamma_{pp}|A_p|^2+2\gamma_{ps}|A_s|^2)A_p-\frac{\sigma_p}{2}(1+i\mu_p)NA_p\\&+i\gamma_p A_s\int_{-\infty}^{t}h(t-t')A_s^*(z,t')A_p(z,t')\,e^{i\Omega_{ps}(t-t')}dt'\end{aligned} \tag{2a}$$

$$\begin{aligned}\frac{\partial A_s}{\partial z}&+\beta_{1s}\frac{\partial A_s}{\partial t}+\frac{i\beta_{2s}}{2}\frac{\partial^2 A_s}{\partial t^2}=-\frac{\alpha_s}{2}A_s\\&+i(\gamma_{ss}|A_s|^2+2\gamma_{sp}|A_p|^2)A_s-\frac{\sigma_s}{2}(1+i\mu_s)NA_s\\&+i\gamma_s A_p\int_{-\infty}^{t}h(t-t')A_p^*(z,t')A_s(z,t')\,e^{i\Omega_{sp}(t-t')}dt'.\end{aligned} \tag{2b}$$

Here, the two time-derivative terms represent the linear dispersion and group velocity dispersion (GVD) characterized by the constants β_{1u} and β_{2u}, respectively.

The notation and physical meaning of different terms on the right-hand side of (2) are as follows. The first term accounts for linear losses through the parameter α_u $(u = p, s)$. The second term is responsible for both the Kerr and TPA processes through the nonlinear parameters

$$\gamma_{uv} = k_{uv} n_2 (1 + i r_{uv}) \quad (u, v = p \text{ or } s)$$
$$r_{uu} = \frac{\beta_{\mathrm{TPA}u}}{2k_u n_2} \qquad r_{uv} = \frac{\beta_{\mathrm{TPA}uv}}{2k_{uv} n_2}$$

where n_2 is the nonlinear Kerr coefficient, $\beta_{\mathrm{TPA}u}$ is the TPA coefficient at frequency ω_u, and $\beta_{\mathrm{TPA}ps} = (\omega_p/\omega_s)\beta_{\mathrm{TPA}sp}$ is the cross-TPA coefficient. Also, $k_{uu} = k_u$ and the parameter k_{uv} $(u \neq v)$ is related to the real part of the third-order electronic susceptibility $\chi^{(3)}(-\omega_u; \omega_v, -\omega_u, \omega_v)$ [12]. The third term in (2) represents the contribution from TPA-generated free carriers through $\sigma_u = \sigma_r(\lambda_u/\lambda_r)^2$. Here, $\sigma_r = 1.45 \times 10^{-21}$ m^2 is the free-carrier absorption (FCA) coefficient at the reference wavelength $\lambda_r = 1550$ nm. Finally, the dimensionless parameter $\mu_u = 2k_u\sigma_n/\sigma_r$ accounts for free-carrier-induced changes in the refractive index with $\sigma_n = 5.3 \times 10^{-27}$ m^3. The form of the TPA terms implies that electrons and holes are not injected into the waveguide but generated optically with equal densities $N(z,t)$.

The integrals in (2) account for SRS whose magnitude depends on the pump-signal frequency detuning $\Omega_{ps} = -\Omega_{sp} = \omega_p - \omega_s$. When the waveguide cross-section area varies along the waveguide length, the Raman nonlinear parameter γ_u becomes a function of the propagation distance such that

$$\gamma_p(z) = \frac{g_R\gamma_R/\Omega_R}{\sqrt{A_{\mathrm{eff}\,p}(z)A_{\mathrm{eff}\,s}(z)}} \qquad \gamma_s(z) = \frac{\omega_s}{\omega_p}\gamma_p(z)$$

where g_R is the Raman gain coefficient, γ_R is the full-width at half-maximum (FWHM) of the Raman gain spectrum (about 105 GHz for silicon), Ω_R is the Raman shift (about 15.6 THz for silicon), and $A_{\mathrm{eff}\,u}(z)$ is the effective mode area (EMA) defined as

$$A_{\mathrm{eff}\,u}(z) = \frac{\left(\iint |F_u(\mathbf{r})|^2 dxdy\right)^2}{\left(\iint |F_u(\mathbf{r})|^4 dxdy\right)}.$$

In the classical oscillator model of SRS [81], the Raman response function $h(t)$ is given by the expression

$$h(t) = \frac{\Omega_R^2}{\Omega_0}\sin(\Omega_0 t)\exp(-\gamma_R t)$$

where $\Omega_0 = (\Omega_R^2 - \gamma_R^2)^{1/2}$.

Equations (2) can be solved if we add another equation describing the evolution of the TPA-induced free carrier density. This equation should include all mechanisms through which free carriers can be generated and all channels through which they can recombine, including radiative recombination, thermal diffusion, and drift of electrons and holes to the waveguide periphery stimulated by an external field. It is common to lump the impact of all recombination channels in a single parameter τ_c, which is called the effective carrier lifetime [12]–[14]. With this simplification, the carrier rate equation becomes

$$\frac{\partial N}{\partial t} = -\frac{N}{\tau_c} + \rho_p|A_p|^4 + \rho_s|A_s|^4 + \rho_{ps}|A_pA_s|^2 \qquad (3)$$

where

$$\rho_u(z) = \frac{\beta_{\mathrm{TPA}u}}{2\hbar\omega_u A_{\mathrm{eff}\,u}^2(z)} \qquad \rho_{ps}(z) = \frac{2\beta_{\mathrm{TPA}ps}}{\hbar\omega_p A_{\mathrm{eff}\,p}(z)A_{\mathrm{eff}\,s}(z)}.$$

We should also note that the field envelopes in (2) are expressed in units of the square root of power. The corresponding mapping functions are

$$s_u(z) = \left[\frac{(\mu_0/\varepsilon_0)^{1/2}}{2n_0 A_{\mathrm{eff}\,u}(z)}\right]^{1/2}$$

where μ_0 is the intrinsic permeability of vacuum.

Due to the presence of intricate cross-coupling terms, it is evident that the system of equations (2) and (3) cannot be solved analytically. Nevertheless, several approximate solutions that could shed light on the nonlinear optics of silicon waveguides can be derived in several cases of immense practical interest. In the following sections, we start with the simplest situation of a single pulse launched into an SOI waveguide, and then, focus on more complicated cases involving two pulses at different wavelengths.

III. Propagation of a Single Signal Pulse

In the simplest scenario, only one optical pulse at the carrier frequency ω_s travels through a waveguide of constant cross section. Then, we can set $A_p = 0$ in (2). If the waveguide length L is much shorter than the dispersion length $L_d = T_0^2/|\beta_{2s}|$, where T_0 is the temporal pulsewidth, then the GVD term in (2) can be ignored. The term containing β_{1s} can be eliminated by introducing $\tau = t - \beta_{1s}z$ as the retarded time in a reference frame moving with the pulse center. With these simplifications, propagation through the SOI waveguide is described by the following two equations [82]:

$$\frac{\partial \mathcal{E}}{\partial z} = -\frac{\alpha_s}{2}\mathcal{E} + \left(ik_s n_2 - \frac{\beta}{2}\right)|\mathcal{E}|^2\mathcal{E} - \frac{\sigma_s}{2}(1 + i\mu_s)N\mathcal{E} \qquad (4a)$$

$$\frac{\partial N}{\partial \tau} = -\frac{N}{\tau_c} + p\,|\mathcal{E}|^4 \qquad (4b)$$

where $\mathcal{E}(z,\tau) = A(z,\tau)/A_{\mathrm{eff}}^{1/2}$ is the electric field envelope (in units of the square root of intensity), A_{eff} is the constant EMA of the mode, and $p = \beta/(2\hbar\omega_s)$. For simplicity of notation, we employ $\beta \equiv \beta_{\mathrm{TPA}s}$ for the TPA parameter.

It is convenient to rewrite (4) in the terms of the auxiliary intensity $I(z,\tau) = |\mathcal{E}(z,\tau)|^2\exp(\alpha_s z)$ [note that the actual intensity of signal is $|\mathcal{E}(z,\tau)|^2$] and the optical phase (defined modulo 2π) $\phi(z,\tau)$ of the pulse envelope. Introducing

$$\mathcal{E}(z,\tau) = \sqrt{I(z,\tau)}\exp\left[-\left(\frac{\alpha_s}{2}\right)z + i\phi(z,\tau)\right]$$

we obtain the following set of three real first-order differential equations:

$$\frac{\partial I}{\partial z} = -\beta\, I^2 e^{-\alpha_s z} - \sigma_s N I \qquad (5a)$$

$$\frac{\partial \phi}{\partial z} = -\sigma_s\frac{\mu_s}{2}N + k_s n_2 I\, e^{-\alpha_s z} \qquad (5b)$$

$$\frac{\partial N}{\partial \tau} = -\frac{N}{\tau_c} + p\, I^2\, e^{-2\alpha_s z}. \qquad (5c)$$

It is important to note that even though (5a) and (5c) are coupled, (5b) does not have such dependency, and hence, can be solved by direct integration once a solution for these coupled equations is found.

A. Effects of TPA on Self-Phase Modulation

Before solving the full set (5), we consider a special case and assume that the free carrier density N is sufficiently small that its impact on the pulse is negligible. In this case, we can ignore (5c) and set $N = 0$ in the remaining two equations, which can now be easily solved with the result

$$I_0(z,\tau) = \frac{\mathcal{I}(\tau)}{1 + \beta \mathcal{I}(\tau) L_{\rm eff}(z)} \tag{6}$$

where $\mathcal{I}(\tau)$ is the intensity profile of the input pulse and $L_{\rm eff}(z)$ is the standard effective propagation length used extensively in the literature and is defined as [12], [36], [83]

$$L_{\rm eff}(z) = \frac{1 - \exp(-\alpha_s z)}{\alpha_s}. \tag{7}$$

The subscript 0 in $I_0(z,\tau)$ denotes that this solution of (5a) is valid for $\sigma_s = 0$.

The next step is to substitute the solution (6) in the phase equation (5b), which can be integrated easily to find the simple solution

$$\phi_0(z,\tau) = \frac{k_s n_2}{\beta} \ln\bigl[1 + \beta \mathcal{I}(\tau) L_{\rm eff}(z)\bigr]. \tag{8}$$

This is an important analytical result showing explicitly how the nonlinear phase shift induced by the process of self-phase modulation (SPM) is affected by TPA that is unavoidable in silicon waveguides [84]. It is easy to verify from (8) that the phase increases linearly in the absence of TPA ($\beta = 0$). As one may expect, TPA reduces the SPM-induced phase shift, and the reduction becomes more severe at higher input intensity levels because of a logarithmic growth of the phase $\phi(z,\tau)$ with an increase in the input intensity. The investigation of SPM-based regeneration in chalcogenide glass fibers suggests this feature for flattening the transfer functions of SOI-based optical regenerators [85].

It is now straightforward to calculate the pulse shape and spectrum at the output of a waveguide of length L. The main point to note is that considerable physical insight is gained by an analytical solution obtained by making a few approximations justifiable under suitable operating conditions.

B. Effects of Free Carriers on Self-Phase Modulation

The main limitation of the preceding analytic solution is that the neglect of free carriers becomes questionable at high input intensities such that $\beta \mathcal{I} L > 1$. It turns out that we can include the free-carrier effects using a perturbative approach. To construct such an approximate solution of (5), we note that (5c) can be solved formally in the form

$$N(z,\tau) = p\, e^{-2\alpha_s z} \int_{-\infty}^{\tau} e^{-(\tau-\tau')/\tau_c} I^2(z,\tau')\, d\tau' \tag{9}$$

where we have assumed that no free carriers exist before the pulse enters the waveguide, which is an assumption justified in practice for a pulse repetition rate R_p such that $R_p \tau_c \ll 1$. Substituting this result into (5a), we obtain a single integro-differential equation for the pulse intensity

$$\frac{\partial I}{\partial z} = -\beta I^2 e^{-\alpha_s z} - \sigma_s p\, I(z,\tau)\, e^{-2\alpha_s z} \int_{-\infty}^{\tau} e^{-(\tau-\tau')/\tau_c} I^2(z,\tau')\, d\tau'. \tag{10}$$

To proceed further, we assume that TPA-generated free carriers modify the temporal shape of the pulse only slightly. Then, (10) can be replaced by

$$\frac{\partial I}{\partial z} \approx -\beta I^2 e^{-\alpha_s z} - \sigma_s p\, I(z,\tau)\, e^{-2\alpha_s z} \int_{-\infty}^{\tau} e^{-(\tau-\tau')/\tau_c} I_0^2(z,\tau')\, d\tau' \tag{11}$$

where $I_0(z,\tau)$ is the solution obtained earlier in (6). We have recently shown that this integro-differential equation can be solved analytically [82]. The resulting solution involves integrals and is given by

$$I(z,\tau) = \frac{I_0(z,\tau)}{1 + \epsilon(z,\tau)} \tag{12}$$

where

$$\epsilon(z,\tau) = I_0(z,\tau) \int_0^z e^{v(z,\tau) - v(z',\tau)} w(z',\tau)\, dz'$$

$$v(z,\tau) = \sigma_s p \int_{-\infty}^{\tau} e^{-(\tau-\tau')/\tau_c} \varphi(z,\tau')\, d\tau'$$

$$w(z,\tau) = \frac{\sigma_s p}{I_0(z,\tau)} e^{-2\alpha_s z} \int_{-\infty}^{\tau} e^{-(\tau-\tau')/\tau_c} I_0^2(z,\tau')\, d\tau'$$

$$\varphi(z,\tau) = I_0(z,\tau)\left[\frac{\alpha_s}{\beta} + \mathcal{I}(\tau)\right] L_{\rm eff}(z) - \frac{\alpha_s}{\beta k_s n_2}\, \phi_0(z,\tau).$$

In the last equation, $\phi_0(z,\tau)$ is the analytical solution obtained earlier in (8) when free-carrier effects were ignored.

An approximate solution of the phase equation (5b) can also be found in the same manner. Substitution of (9) into (5b) gives

$$\frac{\partial \phi}{\partial z} \approx k_s n_2 \sqrt{I}\, e^{-\alpha_s z} - \mu_s \frac{\sigma_s}{2}\, p\, e^{-2\alpha_s z} \int_{-\infty}^{\tau} e^{-(\tau-\tau')/\tau_c} I_0^2(z,\tau')\, d\tau'.$$

The solution of this equation can be written in the form

$$\phi(z,\tau) = k_s n_2 \int_0^z I(z',\tau)\, e^{-\alpha_s z'} dz' - \frac{\mu_s}{2}\, v(z,\tau). \tag{13}$$

It is easy to verify that, in the absence of free carriers or when $\sigma_s = 0$, these expressions for pulse intensity and phase reduce to the results obtained earlier in [84] and given in (6) and (8).

C. SPM-Induced Spectral Broadening

Equations (9), (12), and (13) provide an approximate solution of the nonlinear system (5) along the SOI waveguide. It is applicable when the influence of free carriers on the pulse intensity is not too strong, i.e., when $\max[\epsilon(z,\tau)] \ll 1$. Several qualitative conclusions can be drawn from the structure of the solution. First, the effects of FCA and free-carrier dispersion (FCD) are cumulative, and thus, appear as the integral functions $w(z,\tau)$ and $v(z,\tau)$, respectively. They are responsible for the asymmetry of the amplitude and phase profiles at the output end even when the input pulse profile is symmetric around the pulse center. Second, as one would expect, the function $\epsilon(z,\tau)$ represents the reduction in the pulse intensity because of FCA. It corresponds to an energy loss experienced by the pulse in addition to that induced by the TPA process. Third, the function $v(z,\tau)$ represents physically the effects of FCD that leads to time-dependent changes in the refractive index. These changes add to the Kerr-induced index changes. Fourth, because $v(z,\tau) > 0$, the nonlinear phase shift due to FCD reduces the Kerr-induced phase shift. Such a reduction can be quite large even when the pulse shape changes slightly because of a relatively large value of the parameter μ_s for silicon (about 7.5) and has interesting consequences for the resulting output pulse spectrum.

To emphasize the last point further, we perform the integral appearing in (13) numerically for three SOI waveguides of different lengths. In each case, the input pulse has the same Gaussian intensity profile $\mathcal{I}(\tau) = \mathcal{I}_0 \exp(-2\tau^2/T_0^2)$ with $T_0 = 10$ ps but the peak intensity $\mathcal{I}_0$ changes from 0.3 to 10 GW/cm^2. The resulting temporal phase profiles are shown in the upper panel of Fig. 1 using parameter values listed there. The dashed curves show for comparison the phase profiles expected in the absence of free-carrier effects. One can see that the free-carrier effects are relatively minor for pulse 3 with a peak intensity of only 0.3 GW/cm^2, but they become very important when peak intensity exceeds 1 GW/cm^2. Note, in particular, that the phase becomes negative near the trailing edge of the pulse because of FCD.

The important question is how the pulse spectrum is modified by such nonlinear phase changes. To answer it, the solid curve in the lower panel of Fig. 1 shows the output spectrum of the most intense pulse with $\mathcal{I}_0 = 10$ GW/cm^2 and compares it with the input spectrum (dotted curve) and the one obtained without free-carrier effects ($\sigma_s = 0$). As expected, SPM-induced spectral broadening in the $\sigma_s = 0$ case leads to a symmetric pulse spectrum. In contrast, the free-carrier effects produce a highly asymmetric spectrum. In agreement with experiments and numerical modeling, the FCD effects broaden the output pulse spectrum and shift it toward shorter wavelengths (the so-called free-carrier-induced blue shift).

It is worth noting that the results of this section can be easily extended to characterize the propagation of an arbitrary pulse train. Indeed, if the function $\mathcal{I}(\tau)$ contains several peaks, it can be thought of as the envelope of a pulse sequence. In this case, applicability of the obtained solution [(9), (12), and (13)] will also depend on the repetition rate of pulses. Particularly, when the pulse-to-pulse spacing becomes comparable to the carrier lifetime, it is necessary to account for a background carrier density in (9) because it does not decay to zero before the next pulse arrives. These residual carriers result in stronger attenuation and broadening of propagating pulses, thereby reducing the applicability domain of our solution.

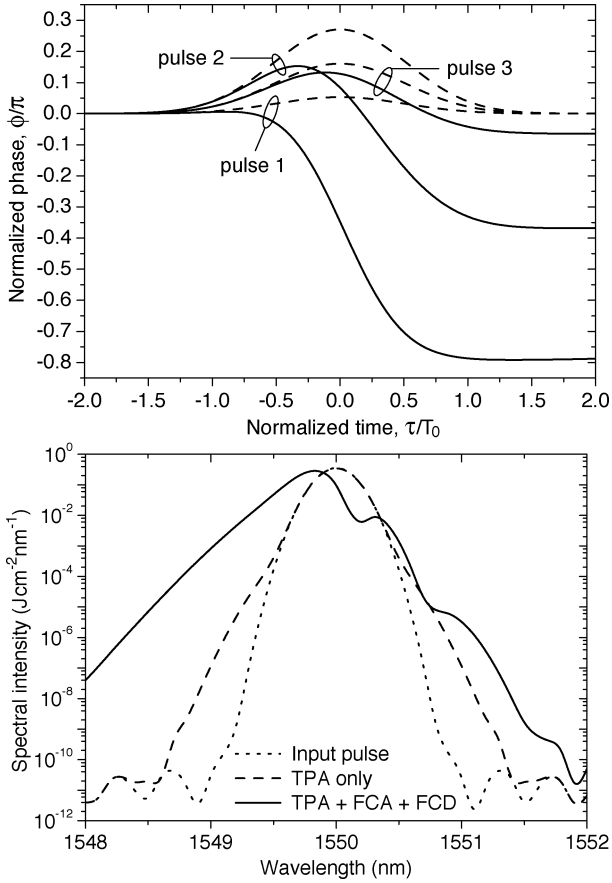

Fig. 1. (Upper panel) Nonlinear phase shifts (solid curves) plotted as a function of time for three input Gaussian pulses. The values of $\mathcal{I}_0$ and L are 10 GW/cm^2 and 70 μm for pulse 1, 1 GW/cm^2 and 4 mm for pulse 2, and 0.3 GW/cm^2 and 8 mm for pulse 3. Dashed curves show phase shifts expected in the absence of FCD. (Lower panel) Output spectrum of pulse 1 (solid curve) broadened by SPM and FCD effects. Dashed curve includes the Kerr and TPA effects but ignores the impact of free carriers. Dotted curve shows for comparison the input pulse spectrum. Parameter values are $\lambda_s = 1550$ nm, $n_0 = 3.484$, $\alpha_s = 1$ dB/cm, $\beta = 5 \times 10^{-12}$ m/W, $n_2 = 6 \times 10^{-18}$ m^2/W, $\tau_c = 1$ ns, and $T_0 = 10$ ps (after [82]).

IV. Single-Pass CW Raman Amplifier

One of the very promising applications of SOI waveguides is related to the amplification of optical signals through SRS. When both the pump and the signal are in the form of CW waves, a valuable analytical solution can be obtained in the case of constant cross-section waveguides. We discuss it in this section as it provides considerable insight into the Raman amplification process.

A. Coupled Intensity Equations

In the CW regime, the envelopes of the pump and signal fields are functions of propagation distance only. As a consequence, all time derivatives in (2) vanish, and the time integrals can be calculated explicitly by noting that

$$\int_{-\infty}^{t} h(t-t')\, e^{\pm i\Omega_{ps}(t-t')} dt' = \frac{\Omega_R^2}{\Omega_R^2 - \Omega_{ps}^2 \pm 2i\gamma_R \Omega_{ps}}.$$

In addition, in the steady-state regime, the free carrier density can be obtained from (3) by setting $\partial N/\partial t = 0$ and is given by

$$N(z) = \tau_c\big(\rho_p |A_p|^4 + \rho_s |A_s|^4 + \rho_{ps} |A_p A_s|^2\big).$$

Using this result in (2) and introducing the intensities of pump and signal (Stokes) waves, $I_p(z) = |A_p(z)|^2/A_{\rm eff}$ and $I_s(z) = |A_s(z)|^2/A_{\rm eff}$, where we assumed that the EMA, $A_{\rm eff}$, is nearly the same for the two waves, we get [86]

$$\begin{aligned}\frac{dI_p}{dz} =& -\alpha_p I_p - \beta_p I_p^2 - \zeta_{ps} I_p I_s \qquad (14a)\\ & - \sigma_p \tau_c (p_p I_p^2 + p_s I_s^2 + p_{ps} I_p I_s) I_p\\ \frac{dI_s}{dz} =& -\alpha_s I_s - \beta_s I_s^2 - \zeta_{sp} I_s I_p\\ & - \sigma_s \tau_c (p_p I_p^2 + p_s I_s^2 + p_{ps} I_p I_s) I_s \qquad (14b)\end{aligned}$$

where we used the following shortened notations:

$$\zeta_{ps} = 2\beta_{ps} + \frac{4 g_R \gamma_R^2 \Omega_R \Omega_{ps}}{(\Omega_R^2 - \Omega_{ps}^2)^2 + 4\gamma_R^2 \Omega_{ps}^2}$$

$$\zeta_{sp} = \frac{\omega_s}{\omega_p}\left(2\beta_{ps} - \frac{4 g_R \gamma_R^2 \Omega_R \Omega_{ps}}{(\Omega_R^2 - \Omega_{ps}^2)^2 + 4\gamma_R^2 \Omega_{ps}^2}\right)$$

$\beta_u = \beta_{{\rm TPA}u}$, $\beta_{ps} = \beta_{{\rm TPA}ps}$, $p_u = \beta_u/(2\hbar\omega_u)$, and $p_{ps} = 2\beta_{ps}/(\hbar\omega_p)$.

In order to solve (14) analytically, we make some reasonable simplifications. First, we assume that linear losses are equal at the pump and signal wavelengths, i.e., $\alpha_p = \alpha_s \equiv \alpha$. Second, we discard second terms on the right side of (14) since TPA is known to be much smaller than FCA in the case of CW pumping [12]. Third, noting that $\Omega_{ps} \approx \Omega_R \ll \omega_{p(s)}$ in practice, we make several rough approximations: $\sigma_p \approx \sigma_s$, $\beta_p \approx \beta_s \approx \beta_{ps} \equiv \beta$, $p_p \approx p_s \approx p_{ps}/4$. Fourth, noting that $g_R \gg \beta_{ps}$ for silicon with $|\Omega_{ps} - \Omega_R| \lesssim \gamma_R$, we use $\zeta_{ps} \approx |\zeta_{sp}| \equiv \gamma$. With these simplifications, the coupled intensity equations (14) become

$$\frac{dI_p}{dz} \approx -\alpha I_p - \kappa (I_p^2 + 4 I_p I_s + I_s^2) I_p - \gamma I_s I_p \qquad (15a)$$

$$\frac{dI_s}{dz} \approx -\alpha I_s - \kappa (I_p^2 + 4 I_p I_s + I_s^2) I_s + \gamma I_p I_s \qquad (15b)$$

where $\kappa \approx \tau_c \sigma_s p_s$.

Finally, we make one more simplification. It consists of replacing the quantity in the parenthesis of (15) with $(I_p + I_s)^2$ and amounts to omitting the terms containing $2\kappa I_p^2 I_s$ and $2\kappa I_s^2 I_p$. After this replacement, we obtain

$$\frac{dI_p}{dz} \approx -\alpha I_p - \kappa (I_p + I_s)^2 I_p - \gamma I_s I_p \qquad (16a)$$

$$\frac{dI_s}{dz} \approx -\alpha I_s - \kappa (I_p + I_s)^2 I_s + \gamma I_p I_s. \qquad (16b)$$

An important point to note is that, even though we drastically approximated (14) to arrive at (16), the simpler equations still qualitatively represent the interplay between the FCA and SRS processes and hold all the basic features of (15).

B. Simple Analytical Solution

Equations (16) can be solved analytically by noting that the total intensity $I(z) = I_p(z) + I_s(z)$ satisfies the Bernoulli equation [87] whose solution is

$$I(z) = \frac{I_0 \exp(-\alpha z)}{\sqrt{1 + \kappa I_0^2 L_{\rm eff}(2z)}}$$

where $I_0 = I_{p0} + I_{s0}$ is the total input intensity with $I_{p0} = I_p(0)$ and $I_{s0} = I_s(0)$. By substituting $I_p(z) = I(z) - I_s(z)$ in (16b), we can solve this equation as well. The resulting solution is given by

$$I_s(z) = \frac{I(z)}{1 + (I_{p0}/I_{s0}) \exp[-\gamma I_0 \mathcal{L}_{\rm eff}(z)]} \qquad (17a)$$

$$I_p(z) = I(z) - I_s(z) \qquad (17b)$$

where the generalized effective length of the waveguide is defined as

$$\mathcal{L}_{\rm eff}(z) = \frac{f(0) - f(z)}{\sqrt{\alpha\kappa}\, I_0}, f(z) = \tan^{-1}\left[\sqrt{\frac{\kappa}{\alpha}}\, I(z)\right].$$

For low input intensities $I_0 \to 0$, FCA becomes negligible. In this limit (or when $\kappa \to 0$), it is easy to show that

$$\mathcal{L}_{\rm eff}(z) \to L_{\rm eff}(z).$$

Equation (17a) shows that changes in the signal intensity result from two sources with different physical origins. The steadily decreasing function $I(z)$ results from linear losses and FCA, whereas the denominator of (17a) arises from SRS and exhibits a saturable character. The structure of the denominator shows that the generalized effective length has direct influence on the signal gain. In the ideal situation, when this length becomes sufficiently large, the signal approaches the total intensity $I(z)$, thus indicating efficient transfer of pump power to the signal.

The influence of FCA on CW Raman amplification manifests in two ways. First, FCA leads to an overall attenuation of the signal as indicated by the radical in the function $I(z)$. Second, it leads to a decrease in the effective length compared to the linear-loss situation only and, what is more important, makes it intensity-dependant. The influence of total input intensity on the generalized effective length is illustrated by solid curves in the upper panel of Fig. 2. Clearly, one can increase $\mathcal{L}_{\rm eff}(z)$ substantially by decreasing I_0. A similar increase in the effective length may be realized by reducing τ_c because κ scales linearly with τ_c.

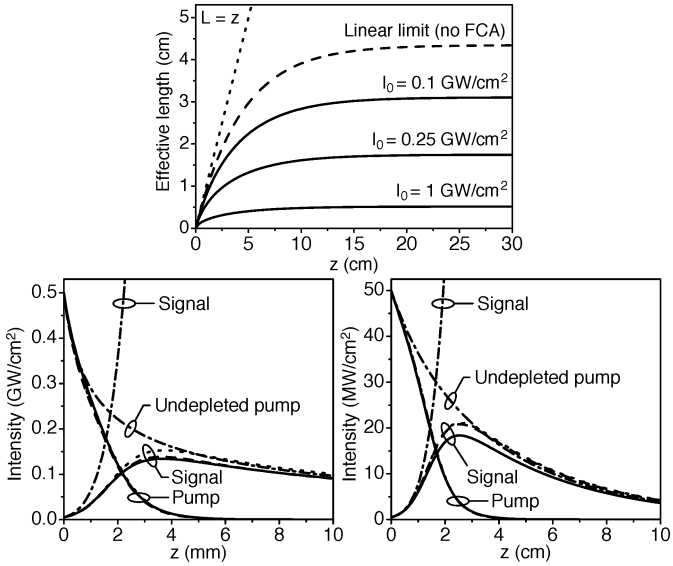

Fig. 2. (Upper panel) Generalized effective length $\mathcal{L}_{\rm eff}(z)$ versus propagation distance for different input intensities I_0 (solid curves). The dashed curve shows the linear-loss limit. The dotted line corresponds to the lossless case. (Lower panel) Evolution of the pump and the signal intensities obtained by solving (14) numerically (solid curves) and predicted analytically by the corrected (dashed curves) and uncorrected (dotted curves) solutions (17). The solution corresponding to the undepleted-pump approximation is shown by dashed-dotted curves. The left and right panels correspond to $I_{p0} = 0.5$ GW/cm^2 and 0.05 GW/cm^2, respectively, with $I_{s0} = 0.01 I_{p0}$. The other parameter values are $\alpha = 1$ dB/cm, $\beta = 0.5$ cm/GW, $\tau_c = 1$ ns, $g_R = 76$ cm/GW, $\lambda_p = 1550$ nm, and $\lambda_s = 1686$ nm (after [86]).

The approximate solution (17) contains errors resulting from the simplifications that were used to get (15) and the terms that we discarded in (16). We can reduce the errors of the second type by introducing correcting multipliers. Assuming a corrected solution of the form

$$I_{s,\rm corr}(z) = \xi(z) I_s(z) \qquad I_{p,\rm corr}(z) = \xi(z) I_p(z)$$

we find from (15) the correcting multiplier

$$\xi(z) = \left(1 + 2\kappa \int_0^z I_p(z') I_s(z')\, dz'\right)^{-1/2}$$

where $I_p(z)$ and $I_s(z)$ are given by (17). Once corrected with this multiplier, (17) provides an analytical solution of (15) that is quite close to the exact numerical solution of (14). The applicability range of this solution can be estimated by considering that the TPA terms in (14) are small compared with the linear-loss or FCA terms when $I_0 \ll \alpha/\beta$ or $I_0 \gg \beta/\kappa$. For $\alpha = 1$ dB/cm, $\beta = 0.5$ cm/GW, and $\lambda_s = 1686$ nm, we obtain $\alpha/\beta \approx 0.5$ GW/cm^2 and $\beta/\kappa \approx 0.01$ GW/cm^2. Thus, the result in (17) is a good approximate solution of (14) for all input intensities. The lower panel of Fig. 2 demonstrates this point by comparing the analytical solution with the exact numerical solution of (14) (solid curves) for two values of input pump powers. The corrected and uncorrected solutions (17) are shown by the dashed and dotted curves, respectively. For reference, the solution that corresponds to the undepleted-pump approximation is also plotted by the dashed-dotted curves.

C. Noise Transfer in Silicon Raman Amplifiers

An important issue for any amplifier is related to the transfer of noise from the pump to the signal. Because of the exponential nature of the Raman amplification, at least during early stages before gain saturation sets in, any intensity noise associated with the pump can be enhanced severely, thus resulting in considerable fluctuation of the amplified signal. The concept of RIN is often employed to quantify this effect. The coupled intensity equations obtained in the preceding section can be used to study the RIN transfer in silicon Raman amplifiers by introducing two time derivatives in (16) as follows:

$$\frac{\partial \mathfrak{I}_p}{\partial z} + \beta_{1p} \frac{\partial \mathfrak{I}_p}{\partial t} \approx -\alpha\, \mathfrak{I}_p - \kappa\, (\mathfrak{I}_p + \mathfrak{I}_s)^2 \mathfrak{I}_p - \gamma\, \mathfrak{I}_s \mathfrak{I}_p \quad (18a)$$

$$\frac{\partial \mathfrak{I}_s}{\partial z} + \beta_{1s} \frac{\partial \mathfrak{I}_s}{\partial t} \approx -\alpha\, \mathfrak{I}_s - \kappa\, (\mathfrak{I}_p + \mathfrak{I}_s)^2 \mathfrak{I}_s + \gamma\, \mathfrak{I}_p \mathfrak{I}_s. \quad (18b)$$

The variables $\mathfrak{I}_p$ and $\mathfrak{I}_s$ are used instead of I_p and I_s to distinguish between the functions of two and one variables.

One fundamental difference between the RIN transfer in fiber Raman amplifiers and that in silicon Raman amplifiers can be clearly seen in (18). Whereas the former occurs only due to SRS, the latter results from both SRS and FCA. This FCA contribution to the RIN transfer results from the nonuniform absorption of the signal by the free carrier density whose small-scale variations result from the noise induced by the pump. Hence, in silicon Raman amplifiers, the RIN transfer may take place even if there is negligible energy exchange between the pump and signal that occurs due to the Raman effect. This happens in practice when the frequency difference between the pump and signal exceeds the Raman shift of 15.6 THz.

Equations (18) are difficult to solve because, in general, the pump and signal travel at different speeds. However, they can be solved easily if we take $\beta_{1p} = \beta_{1s} \equiv \beta_1$ that amounts to assuming the same group velocity for the pump and signal waves. Since we exclude the "walk-off" effects with this assumption, the following analysis does not provide the dependance of RIN transfer on noise frequency. However, this is not a serious limitation because of the relatively small length of SOI waveguides in practice. According to numerical simulations in [88], such an approximation is valid for frequencies below 100 GHz in a typical waveguide. If we introduce a reduced time $\tau = t - \beta_1 z$, the time-derivative terms in (18) disappear, and these two equations reduce to those in (16) with the only difference that the intensities $\mathfrak{I}_p$ and $\mathfrak{I}_s$ depend both on z and τ. Because of this feature, we can use the analytic solution given in (17). More specifically, the solution of (18) with the boundary conditions

$$\mathfrak{I}_p(0,t) = I_{p0} f(t) \qquad \mathfrak{I}_s(0,t) = I_{s0} = \text{const}$$

where $f(t)$ is a function representing noise, is given by (17) with the replacement

$$I_{p0} \rightarrow I_{p0} f(t - \beta_1 z).$$

It is common to model the intensity noise as a weak sinusoidal modulation of the pump at a specific frequency [89]

$$f(t) = 1 + a_m \sin(\omega_m t)$$

where $a_m \ll 1$ is the modulation amplitude and ω_m is the modulation frequency. Using this representation, we expand the solution $\mathfrak{I}_s(z,t)$ as a Taylor series in the parameter a_m and retain only the first two terms in the series to obtain the following expression for the relative variation of signal gain in the presence of noise:

$$\frac{\delta\mathfrak{G}(z,t)}{G(z)} = \frac{\mathfrak{I}_s(z,t)}{I_s(z)} - 1 \approx a_m \Re(z) \sin[\omega_m (t - \beta_1 z)]$$

where $\mathfrak{G}(z,t) = \mathfrak{I}_s(z,t)/I_{s0}$ and $G(z) = I_s(z)/I_{s0}$ are the signal gains in the presence and absence of noise, respectively, and the noise enhancement factor $\Re(z)$ is given by

$$\Re(z) = \frac{I_{p0}/I_0}{1 + \kappa I_0^2 L_{\text{eff}}(2z)} - \frac{I_p(z)}{I(z)} \left[1 - I_{p0} \frac{\gamma}{\alpha} \frac{1 - I(z)/I_0}{1 + \kappa I_0^2/\alpha}\right].$$

According to its definition, the signal RIN $r_s(z)$ is the square of relative intensity variations averaged over a fairly large time interval. In our case, it suffices to carry out the averaging over a period of noise oscillations $T_m = 2\pi/\omega_m$. The result is

$$r_s(z) = \frac{1}{T_m} \int_0^{T_m} \left[\frac{\delta\mathfrak{G}(z,t)}{G(z)}\right]^2 dt = \frac{a_m^2}{2} \Re^2(z).$$

The RIN on pump can be calculated similarly

$$r_p(z) = \frac{1}{T_m} \int_0^{T_m} \left[\frac{\mathfrak{I}_p(z,t)}{I_p(z)} - 1\right]^2 dt = \frac{a_m^2}{2}.$$

Using the last two equations, we arrive at the following expression for RIN transfer in CW silicon Raman amplifiers:

$$R(z) = \frac{r_s(z)}{r_p(z)} = \Re^2(z). \tag{19}$$

The RIN transfer calculated with (19) is plotted in Fig. 3 together with the average signal intensity. The solid and dashed-dotted-dotted curves represent the RIN transfer under the operating conditions used in the lower panel of Fig. 2 (in both cases, $\tau_c = 1$ ns). The results show that the RIN transfer grows with propagation distance when the pump intensity is sufficiently high, reaches a maximum value just before the signal peaks, and starts decaying when pump intensity becomes low. The decaying occurs because of signal smoothing caused by the intensity-dependant FCA. When the signal intensity becomes low enough to make FCA negligible, the extent of RIN transfer reaches a constant value.

The situation becomes more intricate in the waveguides with a longer free-carrier lifetime. As an example, dashed, dotted, and dotted-dashed curves in Fig. 3 show how the situation changes for $\tau_c = 2$, 3, and 4 ns, respectively. All other parameters are equal to those used for the solid curve. One can see that, at some distance within the waveguide, the magnitude of RIN transfer from the pump to the signal takes large negative values on the decibel scale, indicating that the signal is much less noisy than the pump. This interesting peculiarity has its origin in the competition between the SRS and FCA effects described quantitatively by the coupled equations in (18).

The mechanism behind RIN compensation can be understood by noting that when τ_c is large, a higher pump power may provide lower signal gain because of stronger FCA (see the upper panel in Fig. 4). As a consequence, near the input end, signal fluctuations are in antiphase with respect to pump intensity fluctuations for $\tau_c = 2$, 3, or 4 ns [$\Re(z) < 0$]. As the total intensity in the waveguide diminishes during propagation, the relative efficiency of FCA decreases and the signal fluctuations become in-phase [$\Re(z) > 0$]. At some point z_s along the waveguide, these two contributions cancel each other, thus resulting in $\Re(z_s) = 0$ and no RIN transfer from the pump to the signal. Using the Taylor series expansion of the noise enhancement factor

$$\Re(z) \approx I_{p0}(\gamma - 2\kappa I_0) z + o(z^2)$$

we can find the critical value of the carrier lifetime τ_{cr} above which the compensation of RIN transfer becomes possible. From the expansion, it follows that τ_{cr} corresponds to $\kappa_{\text{cr}} = \gamma/(2I_0)$, i.e.,

$$\tau_{\text{cr}} \approx \frac{\kappa_{\text{cr}}}{\sigma_s p_s} = \frac{\gamma \hbar \omega_s}{I_0 \sigma_s \beta_s}.$$

In the case of Fig. 3, $I_0 = 505$ MW/cm^2 and $\tau_{\text{cr}} = 1.89$ ns, which is a value consistent with our results.

It is interesting to note that, due to the possibility of a self-cancelation effect, if the device parameters are carefully chosen, RIN transfer between the pump and the signal can be made negligible without affecting the overall signal gain. This can be seen from the lower panel in Fig. 3 where the maximum

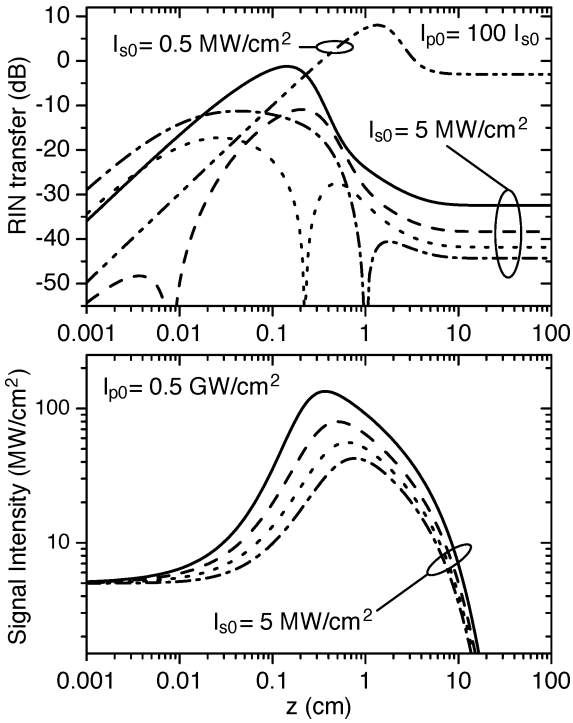

Fig. 3. (Upper panel) RIN transfer and (lower panel) average signal intensity as a function of propagation distance for $\tau_c = 1$ ns (solid curves), 2 ns (dashed curves), 3 ns (dotted curves), and 4 ns (dashed-dotted curves). Solid and dashed-dotted-dotted curves represent the RIN transfer from the pump to the signal shown in the lower panel of Fig. 2. For other curves, parameter values correspond to those used in the lower left panel of Fig. 2.

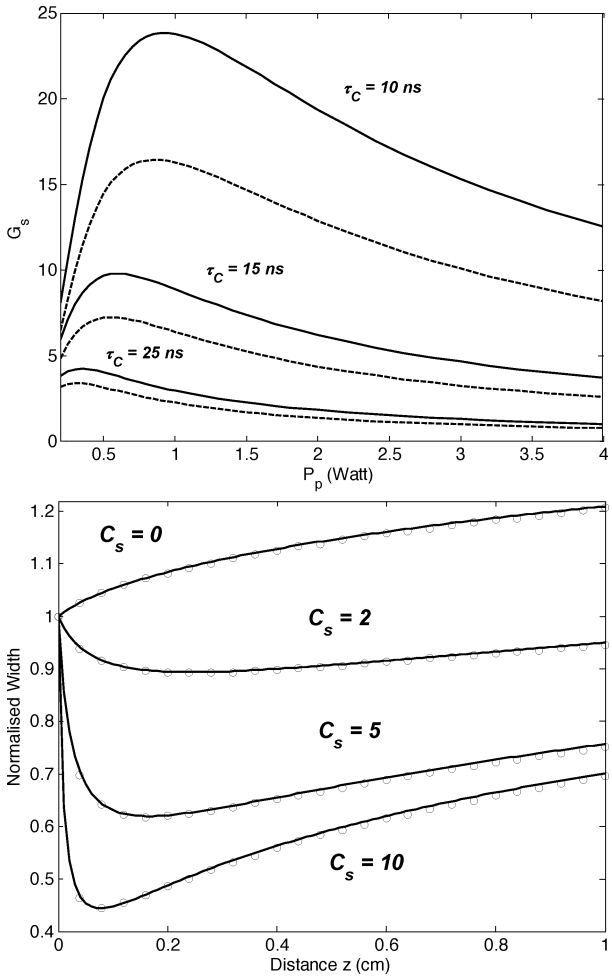

Fig. 4. (Upper panel) Amplification factor plotted as a function of launched pump power for three values of τ_c. Solid curves correspond to $T_2 = 0$ (infinite gain bandwidth) whereas $T_2 = 3$ ps for dashed curves (105 GHz bandwidth). (Lower panel) Evolution of pulsewidth with z for several values of initial chirping. Open circles represent the corresponding values obtained numerically. The simulation parameters are $L = 1$ cm, $\alpha_s = 1$ dB/cm, $\beta = 0.5$ cm/GW, $n_2 = 6 \times 10^{-18}$ m^2/W, $g_R = 76$ cm/GW, $\tau_c = 10$ ns, $\beta_{2s} = 20$ ps^2/m, $\mu = 7.5$, $\lambda_s = 1550$ nm, $T_s = 10$ ps, $T_2 = 3$ ps, $I_p(0) = 250$ MW/cm^2, and $I_s(0) = 0.25$ MW/cm^2 (after [90]).

of the signal intensity (at $z \approx 1$ cm) occurring for $\tau_c = 4$ ns nearly coincides with the dip in the corresponding RIN transfer function shown in the upper panel of the same figure. Hence, the effect of RIN transfer compensation can be realized in SOI-based, gain-optimized, Raman amplifiers with a suitable design.

V. Raman Amplification of Ultrashort Pulses

So far, we have ignored dispersive effects by assuming either a CW situation or relatively broad pulses for which the dispersion length far exceeds the waveguide length. In this section, we focus on the Raman amplification of short pulses for which the dispersive effects cannot be neglected. To keep the analysis simple, we still assume a CW pump that is sufficiently strong to remain nearly undepleted [89]. In this case, a variational formalism allows one to derive a set of relatively simple, first-order, coupled differential equations [90] that describe the evolution of pulse parameters and provide considerable physical insight for designing SOI-based Raman amplifiers. Since this set of equations must be solved numerically, we call this method semianalytical. The main point to stress is that the numerical solution of these equations can be obtained much faster than the original equations and it provides direct information about changes in the amplitude, phase, width, and chirp of the pulse during the Raman amplification process.

The starting point again is the the set of three coupled equations (2) and (3), but we simplify them with the following approximations. First, assuming that the pump is much stronger than the signal, we discard all the terms with A_s in (2a) and (3). Further, because we assume a CW pump, we neglect the dispersion terms in (2a). As a result, the amplitude of the CW pump and the density of free carriers depend only on z. Finally, limiting our attention to the vicinity of the Raman frequency, i.e., assuming that $\Omega_{ps} \approx \Omega_R$, we simplify the last term (denoted by T_R) in (2a) containing an integral over the Raman response function as follows:

$$T_R = i\gamma_s |A_p(z)|^2 \int_0^\infty h(t') A_s(z, t-t')\, e^{i\Omega_{sp} t'} dt'$$
$$\approx \gamma_R \frac{g_R}{2} |\mathcal{E}_p(z)|^2 \int_0^\infty e^{i(\Omega_{sp}-\Omega_R)t' - \gamma_R t'} \mathcal{E}_s(z, t-t')\, dt'$$

where $\mathcal{E}_u = A_u / A_{\text{eff}}^{1/2}$ $(u = p, s)$. Here, we assumed that $\Omega_0 \approx \Omega_R$, $\omega_s \approx \omega_p$, and left only the resonant term in the Raman response function. Taking the Fourier transform ($\mathcal{F}$) of this expression and assuming $|\omega + \Omega_{sp} - \Omega_R| \ll \gamma_R$, we obtain

$$\mathcal{F}(T_R) \approx \frac{g_R}{2} \frac{|\mathcal{E}_p(z)|^2 \mathcal{E}_s(z, \omega)}{1 - i(\omega + \Omega_{sp} - \Omega_R)/\gamma_R}.$$

This equation explicitly shows the frequency dependence of the Raman susceptibility. We use the condition $\Omega_{sp} \approx \Omega_R$, a prerequisite for Raman amplification to take place, expand the result in a Taylor series assuming $\omega \ll \gamma_R$, retain first three terms, and take the inverse Fourier transform. The result is

$$T_R \approx \frac{g_R}{2} |\mathcal{E}_p(z)|^2 \left[\mathcal{E}_s(z,t) + \frac{1}{\gamma_R} \frac{\partial \mathcal{E}_s}{\partial t} + \frac{1}{\gamma_R^2} \frac{\partial^2 \mathcal{E}_s}{\partial t^2} \right].$$

The first-derivative term provides a small correction to the group velocity and can be neglected in practice.

With the preceding simplifications, we can rewrite (2) using the retarded time $\tau = t - \beta_{1s} z$ and the steady-state solution of the carrier density equation (3) as follows:

$$\frac{d\mathcal{E}_p}{dz} = -\frac{\alpha_p}{2} \mathcal{E}_p - \frac{\kappa_{pp}}{2}(1 + i\mu)|\mathcal{E}_p|^4 \mathcal{E}_p + ik_p n_2 (1 + ir)|\mathcal{E}_p|^2 \mathcal{E}_p \quad (20a)$$

$$\frac{\partial \mathcal{E}_s}{\partial z} + \frac{i\beta_{2s}}{2} \frac{\partial^2 \mathcal{E}_s}{\partial \tau^2} = -\frac{\alpha_s}{2} \mathcal{E}_s - \frac{\kappa_{sp}}{2}(1 + i\mu)|\mathcal{E}_p|^4 \mathcal{E}_s + ik_s n_2 (1 + ir)(|\mathcal{E}_s|^2 + 2|\mathcal{E}_p|^2)\mathcal{E}_s + \frac{g_R}{2}\left(1 + T_2^2 \frac{\partial^2}{\partial \tau^2}\right)|\mathcal{E}_p|^2 \mathcal{E}_s \quad (20b)$$

where $\kappa_{pp} = \tau_c \sigma_p \beta / (2\hbar\omega_p)$, $\kappa_{sp} = \tau_c \sigma_s \beta / (2\hbar\omega_p)$, $\mu = 2k_s \sigma_n / \sigma_r$, $r = \beta/(2k_s n_2)$, and $T_2 = 1/\gamma_R$.

It is important to note that the signal equations do not depend on the pump phase because the Raman amplification process is driven only by the pump intensity $I_p(z) = |\mathcal{E}_p(z)|^2$. From (20a), $I_p(z)$ satisfies the simple equation

$$\frac{dI_p}{dz} = -\alpha_p I_p - \beta I_p^2 - \kappa_{pp} I_p^3$$

with the implicit solution of the form

$$-\alpha_p z = \ln\frac{I_p(z)}{I_p(0)} + \frac{1}{2}\ln\frac{\alpha_p + \beta I_p(0) + \kappa_{pp} I_p^2(0)}{\alpha_p + \beta I_p(z) + \kappa_{pp} I_p^2(z)} + Q\left\{\tan^{-1}[QK(0)] - \tan^{-1}[QK(z)]\right\}$$

provided $4\alpha_p\kappa_{pp} > \beta^2$. Here, $Q = (4\alpha_p\kappa_{pp}/\beta^2 - 1)^{-1/2}$ and $K(z) = 1 + 2(\kappa_{pp}/\beta)I_p(z)$. This solution is employed to solve the signal equation (20b).

An approximate solution of the signal equation can be obtained with a variational technique that makes use of a Rayleigh dissipation function (RDF) to account for signal losses along the waveguide [90]. More specifically, we introduce the Lagrangian and the RDF as

$$\mathcal{L} = \frac{1}{2}\left(\mathcal{E}_s\frac{\partial\mathcal{E}_s^*}{\partial z} - \mathcal{E}_s^*\frac{\partial\mathcal{E}_s}{\partial z}\right) + \frac{i\beta_{2s}}{2}\left|\frac{\partial\mathcal{E}_s}{\partial\tau}\right|^2 + \frac{ik_s n_2}{2}(|\mathcal{E}_s|^2 + 4I_p)|\mathcal{E}_s|^2 - \frac{i\mu\kappa_{sp}}{2}I_p^2|\mathcal{E}_s|^2 \quad (21)$$

and

$$\mathcal{R} = \frac{1}{2}\left[\alpha_s + \beta(|\mathcal{E}_s|^2 + 2I_p) - g_R I_p + \kappa_{sp} I_p^2\right] \times \left(\mathcal{E}_s\frac{\partial\mathcal{E}_s^*}{\partial z} - \mathcal{E}_s^*\frac{\partial\mathcal{E}_s}{\partial z}\right) - \frac{g_R}{2}T_2^2 I_p\left(\frac{\partial^2\mathcal{E}_s}{\partial\tau^2}\frac{\partial\mathcal{E}_s^*}{\partial z} - \frac{\partial^2\mathcal{E}_s^*}{\partial\tau^2}\frac{\partial\mathcal{E}_s}{\partial z}\right). \quad (22)$$

We assume that the signal pulse launched into a silicon waveguide has a Gaussian shape and it maintains this shape during Raman amplification even though its parameters change and evolve with z. Thus, the signal field has the form

$$\mathcal{E}_s(z,\tau) = \sqrt{I_s(z)}\exp\left\{-[1 - ic_s(z)]\frac{\tau^2}{2T_s^2(z)} + i\varphi_s(z)\right\}$$

where I_s, c_s, T_s, and φ_s represent, respectively, the peak intensity, frequency chirp, width, and phase of the signal pulse. Inserting this expression in (21) and (22), we can calculate the reduced Lagrangian and the RDF defined as

$$\mathcal{L}_g(z) = \int_{-\infty}^{\infty}\mathcal{L}(z,\tau)\,d\tau \qquad \mathcal{R}_g(z) = \int_{-\infty}^{\infty}\mathcal{R}(z,\tau)\,d\tau$$

because time integrals can be done analytically. Employing the Euler equation

$$\frac{d}{dz}\left(\frac{\partial\mathcal{L}_g}{\partial q_z}\right) - \frac{\partial\mathcal{L}_g}{\partial q} = -\frac{\partial\mathcal{R}_g}{\partial q_z}$$

where $q = \{I_s, c_s, T_s, \varphi_s\}$ and $q_z = dq/dz$, we arrive at the following set of four ordinary differential equations for the pulse parameters [90]:

$$\frac{dI_s}{dz} = -(\alpha_s + 2\beta I_p)I_s + g_R\left(1 - \frac{T_2^2}{T_s^2}\right)I_p I_s + \beta_{2s}\frac{c_s}{T_s^2}I_s - \frac{5\beta}{4\sqrt{2}}I_s^2 - \kappa_{sp}I_p^2 I_s \quad (23a)$$

$$\frac{dT_s}{dz} = -\beta_{2s}\frac{c_s}{T_s} + \frac{\beta}{4\sqrt{2}}T_s I_s + \frac{g_R}{2}\frac{T_2^2}{T_s}(1 - c_s^2)I_p \quad (23b)$$

$$\frac{dc_s}{dz} = -\frac{\beta_{2s}}{T_s^2}(1 + c_s^2) - \frac{k_s n_2}{\sqrt{2}}I_s + \frac{\beta}{2\sqrt{2}}c_s I_s - g_R\frac{T_2^2}{T_s^2}(1 + c_s^2)c_s I_p \quad (23c)$$

$$\frac{d\varphi_s}{dz} = \frac{\beta_{2s}}{2T_s^2} + \frac{5k_s n_2}{4\sqrt{2}}I_s - \frac{\mu\kappa_{sp}}{2}I_p^2 + \left(2k_s n_2 + \frac{g_R}{2}\frac{T_2^2}{T_s^2}c_s\right)I_p. \quad (23d)$$

These equations determine the evolution of the signal pulse during Raman amplification. By looking at their structure, one can understand physically which nonlinear phenomenon affects which pulse parameters. For example, the presence of the gain dispersion parameter T_2 in (23a)–(23c) explicitly shows that gain dispersion affects pulse amplitude, width, and chirp, and thus, plays a significant role when pulsewidth is comparable to T_2. Since $T_2 = 3$ ps for silicon, gain dispersion effects become negligible for $T_s > 30$ ps but cannot be neglected for pulsewidths close to 10 ps or less.

In practice, the evolution of pulse intensity I_s along the waveguide is of primary interest as it governs the extent of Raman amplification. Typically, the input intensity of the pump is much higher than that of the signal. As a result, in the vicinity of the waveguide input, TPA caused by the signal is relatively small and we can safely drop the I_s^2 term in (23a). The amplification of the signal is possible only if $dI_s/dz > 0$, or

$$\kappa_{sp}I_p^2 - \left[g_R\left(1 - \frac{T_2^2}{T_s^2}\right) - 2\beta\right]I_p + \alpha_s - \beta_{2s}\frac{c_s}{T_s^2} < 0.$$

If $\alpha_s T_s^2 > \beta_{2s}c_s$, this quadratic equation and the requirement that pump intensity is a real positive quantity lead to the following limitation on the carrier lifetime [90]:

$$\tau_c < \tau_{\rm th} \equiv \frac{\left[g_R(1 - T_2^2/T_s^2) - 2\beta\right]^2}{4\sigma_s p_p(\alpha_s - \beta_{2s}c_s/T_s^2)}. \quad (24)$$

Equation (24) shows that the carrier lifetime should be less than a threshold value $\tau_{\rm th}$ before CW pumping can be used for Raman amplification of a signal pulse. Note that both the waveguide dispersion and pulse chirp affect $\tau_{\rm th}$ through their sign function $\mathrm{sgn}(\beta_{2s}c_s)$. In particular, $\tau_{\rm th}$ is reduced when $\beta_{2s}c_s$ becomes negative. On the other hand, if $\beta_{2s}c_s > 0$, the threshold value can be made relatively high. Also note that the restriction on τ_c disappears altogether for $\beta_{2s}c_s > \alpha_s T_s^2$. These conclusions are quite important for Raman amplification of picosecond

pulses in silicon waveguides and show why simple analytic tools are essential for understanding nonlinear phenomena in such devices.

As an example, we consider Raman amplification of 10-ps Gaussian pulses in a 1-cm-long SOI waveguide and solve coupled equations (23a)–(23c) numerically. The upper panel in Fig. 4 shows the amplification factor $G_s = P_s(L)/P_s(0)$ as a function of input pump power for $T_2 = 0$ (solid curves) and $T_2 = 3$ ps (dashed curves) for three values of the carrier lifetime τ_c. The Raman gain bandwidth is very large in the former case but corresponds to the realistic value of 105 GHz in the latter case. In all cases, an increase in the pump power does not always enhance the signal gain; rather, after a certain value of input pump power, the effective signal gain starts to decrease. This feature can be attributed to an increase in TPA and the resulting FCA with increasing pump powers. The important point to note is that G_s is reduced considerably for 10-ps pulses because of a relatively narrow Raman gain bandwidth. For example, the maximum value of G_s is reduced from 24 to 16 when carrier lifetime is 10 ns. We also find that G_s is reduced for chirped pulses because of an increased spectral bandwidth for them. The lower panel of Fig. 4 shows how the width of pulses being amplified changes along the waveguide. Although unchirped input pulses always broaden because of gain dispersion, chirped pulses go through an initial compression stage. The width reduction occurs because the central part of a linearly chirped pulse experiences more amplification compared with its pedestals. Numerical results (shown by circles), which are obtained by solving the full model, support the narrowing of chirped pulses.

VI. Raman Amplification in Tapered Waveguides

As a last example of the usefulness of analytic tools, we consider Raman amplification inside a tapered waveguide and ask if there is an optimum tapering profile that will maximize the net signal amplification. To keep the problem tractable, we assume that both the pump and the signal are in the form of CW or quasi-CW waves so that dispersive effects are negligible. It is known that the net gain of silicon Raman amplifiers can be altered by tapering a waveguide along its length [47], [48], [52]. The principle behind tapering consists of balancing of FCA and SRS processes inside the waveguide by varying its lateral dimensions. Such a balancing is possible due to the fact that FCA and SRS terms in (2) have different dependance on EMA.

To find the optimal tapering profile of the SOI waveguide, we convert the set (2) of coupled-amplitude equations into one dealing with the pump and signal powers by using $P_p(z) = |A_p(z)|^2$, $P_s(z) = |A_s(z)|^2$, and following the same procedure used earlier for deriving (14). The result is [91]

$$\frac{dP_p}{dz} = -\alpha_p P_p - \beta_p \frac{P_p^2}{A_{\rm eff}} - \zeta_{ps}\frac{P_p P_s}{A_{\rm eff}} - \sigma_p \tau_c (p_p P_p^2 + p_s P_s^2 + p_{ps} P_p P_s)\frac{P_p}{A_{\rm eff}^2} \tag{25a}$$

$$\frac{dP_s}{dz} = -\alpha_s P_s - \beta_s \frac{P_s^2}{A_{\rm eff}} - \zeta_{sp}\frac{P_s P_p}{A_{\rm eff}} - \sigma_s \tau_c (p_p P_p^2 + p_s P_s^2 + p_{ps} P_p P_s)\frac{P_s}{A_{\rm eff}^2} \tag{25b}$$

where we assumed that the EMA, $A_{\rm eff}$, is the same for the pump and signal beams. The EMA is related to the waveguide cross section and can be changed by tapering the waveguide width. To account for tapering, we allow $A_{\rm eff}$ to vary with z. Note that equations (25) cannot be written in the form of coupled intensity equations (14) when $A_{\rm eff}$ varies with z.

In the undepleted-pump approximation, the optimal EMA profile that maximizes the output signal power for a given input pump power can be found analytically [47]. When the pump power depletion takes place during amplification, the problem of EMA profile optimization can be reduced to a boundary-value problem for the pump and signal powers and two auxiliary functions introduced judiciously [91]. In this case, the input (or output) waveguide cross section need to be kept fixed at a given value. In this section, we consider the optimization process in more detail.

A. Single-Pass Amplifier: Undepleted-Pump Approximation

When the pump is much stronger than the signal, equations (25) can be simplified to take the form

$$\frac{d\ln P_p}{dz} \approx -\alpha_p - \beta_p I_p(z) - \kappa_{pp} I_p^2(z) \tag{26a}$$

$$\frac{d\ln P_s}{dz} \approx -\alpha_s + |\zeta_{sp}| I_p(z) - \kappa_{sp} I_p^2(z) \tag{26b}$$

where $I_p(z) = P_p(z)/A_{\rm eff}(z)$.

It follows from (26b) that, at the end of the amplifier ($z = L$), the signal gain $G = P_s(L)/P_s(0)$ depends on the value of the integral

$$\int_0^L \left[|\zeta_{sp}| - \kappa_{sp} I_p(z)\right] I_p(z)\, dz$$

peaking at a constant pump intensity $\Im_p = |\zeta_{sp}|/(2\kappa_{sp})$. Thus, the maximal signal gain is achieved when the pump power varies in proportion to the EMA. As is easy to see from (26a), the dependence of the pump power and EMA on z in this case takes the exponential form and are given by

$$P_p(z) = P_p(0)\exp(-qz)$$

$$A_{\rm eff}(z) = A_{\rm eff}(0)\exp(-qz)$$

with $q = \alpha_p + \beta_p \Im_p + \kappa_{pp}\Im_p^2$ and $A_{\rm eff}(0) = P_p(0)/\Im_p$. The resulting signal gain grows exponentially with the length of the waveguide

$$G = \exp[(\kappa_{sp}\Im_p^2 - \alpha_s)L].$$

Clearly, the previous solution will remain valid until

$$L \ll \frac{\ln[P_p(0)/P_s(0)]}{\alpha_p - \alpha_s + \beta_p \Im_p + (\kappa_{pp} + \kappa_{sp})\Im_p^2}.$$

B. Single-Pass Amplifier: General Case

To maximize the net gain of signal at the end of the waveguide in the general case, we should maximize the functional

$$F(A_{\rm eff}) = \int_0^L \frac{1}{P_s}\frac{dP_s}{dz}\,dz = \int_0^L \mathcal{G}(z, A_{\rm eff})\,dz$$

where, according to (25b), the local gain coefficient $\mathcal{G}(z, A_{\rm eff})$ is given by

$$\mathcal{G}(z, A_{\rm eff}) = -\alpha_s - \beta_s \frac{P_s(z)}{A_{\rm eff}(z)} - \zeta_{sp}\frac{P_p(z)}{A_{\rm eff}(z)} - \sigma_s\tau_c\frac{p_p P_p^2(z) + p_s P_s^2(z) + p_{ps}P_p(z)P_s(z)}{A_{\rm eff}^2(z)}.$$

To maximize $F(A_{\rm eff})$, we utilize a standard technique known as calculus of variations [91], [92]. Let $A_{\rm eff}(z)$ be the EMA axial profile for which F is stationary. Equating the variation δF to zero with respect to three variables P_p, P_s, and $A_{\rm eff}$, we obtain the relation

$$\int_0^L (\mathcal{A}\delta P_p + \mathcal{B}\delta P_s)\,dz = \int_0^L \mathcal{C}\delta A_{\rm eff}\,dz \tag{27}$$

where δP_p, δP_s, and $\delta A_{\rm eff}$ represent small axial variations, and we have introduced

$$\mathcal{A} = \frac{1}{A_{\rm eff}}\left(\zeta_{sp} + \sigma_s\tau_c\frac{2p_pP_p + p_{ps}P_s}{A_{\rm eff}}\right)$$

$$\mathcal{B} = \frac{1}{A_{\rm eff}}\left(\beta_s + \sigma_s\tau_c\frac{2p_sP_s + p_{ps}P_p}{A_{\rm eff}}\right)$$

$$\mathcal{C} = \frac{\beta_s P_s + \zeta_{sp}P_p}{A_{\rm eff}^2} + 2\sigma_s\tau_c\frac{p_pP_p^2 + p_sP_s^2 + p_{ps}P_pP_s}{A_{\rm eff}^3}.$$

One more relation among δP_p, δP_s, and $\delta A_{\rm eff}$ can be found by varying P_p and P_s in (25) by a small amount around fixed values. The result is

$$\frac{d(\delta P_p)}{dz} = -a_p\delta P_p - b_s\delta P_s + c_p\delta A_{\rm eff} \tag{28a}$$

$$\frac{d(\delta P_s)}{dz} = -a_s\delta P_s - b_p\delta P_p + c_s\delta A_{\rm eff} \tag{28b}$$

where $b_p = \mathcal{A}P_s$, $c_p = \mathcal{C}P_p$, and a_p is defined as

$$a_p = \alpha_p + 2\beta_p\frac{P_p}{A_{\rm eff}} + \zeta_{ps}\frac{P_s}{A_{\rm eff}} + \sigma_p\tau_c\frac{3p_pP_p^2 + p_sP_s^2 + 2p_{ps}P_pP_s}{A_{\rm eff}^2}.$$

The coefficients a_s, b_s, and c_s are obtained from a_p, b_p, and c_p by interchanging subscripts $p \rightleftarrows s$ and assuming that $p_{sp} = p_{ps}$.

To express the optimal EMA profile $A_{\rm eff}(z)$ in terms of the pump and signal powers, we introduce two auxiliary functions $\varphi(z)$ and $\psi(z)$. Multiplying (28a) by φ, (28b) by ψ, and integrating the resulting equations with respect to z from 0 to L, we obtain

$$\int_0^L \varphi\frac{d(\delta P_p)}{dz}\,dz = \varphi\,\delta P_p\Big|_0^L - \int_0^L \varphi'\delta P_p\,dz = -\int_0^L \varphi\,(a_p\delta P_p + b_s\delta P_s - c_p\delta A_{\rm eff})\,dz$$

$$\int_0^L \psi\frac{d(\delta P_s)}{dz}\,dz = \psi\,\delta P_s\Big|_0^L - \int_0^L \psi'\delta P_s\,dz = -\int_0^L \psi\,(a_s\delta P_s + b_p\delta P_p - c_s\delta A_{\rm eff})\,dz$$

where $\varphi' = d\varphi/dz$ and $\psi' = d\psi/dz$.

Assuming that the boundary conditions at $z = 0$ are fixed (often the case in practice), we set $\delta P_p(0) = \delta P_s(0) = 0$. Since the variational solution should maximize the signal power at $z = L$, $\delta P_s(L) = 0$ as well. Because of these constraints, we do not need to set the boundary values for the auxiliary function ψ. However, we can simplify the algebra considerably by choosing $\varphi(L) = 0$. With this choice, the preceding two equations reduce to

$$\int_0^L \left[(\varphi a_p - \varphi')\,\delta P_p + \varphi\,b_s\delta P_s\right]dz = \int_0^L \varphi c_p\delta A_{\rm eff}\,dz$$

$$\int_0^L \left[\psi b_p\delta P_p + (\psi a_s - \psi')\,\delta P_s\right]dz = \int_0^L \psi c_s\delta A_{\rm eff}\,dz.$$

Adding these equations, we finally obtain the relation

$$\int_0^L \left[(\varphi a_p + \psi b_p - \varphi')\delta P_p + (\psi a_s + \varphi b_s - \psi')\delta P_s\right]dz = \int_0^L (\varphi c_p + \psi c_s)\,\delta A_{\rm eff}\,dz. \tag{29}$$

A comparison of (27) and (29) shows that the optimal EMA of the SOI waveguide can be found from a simple relation

$$\varphi c_p + \psi c_s = \mathcal{C} \tag{30}$$

if the two auxiliary functions satisfy the differential equations

$$\varphi' = a_p\varphi + b_p\psi - \mathcal{A} \tag{31a}$$

$$\psi' = a_s\psi + b_s\varphi - \mathcal{B}. \tag{31b}$$

Equation (30) can be solved easily to provide the following relation:

$$A_{\rm eff}(z) = \frac{2\tau_c[\sigma_s(1 - \psi P_s) - \sigma_p\varphi P_p]}{\varphi P_p Q_{ps} - (1 - \psi P_s)Q_{sp}}\,\mathcal{P} \tag{32}$$

where $Q_{uv} = \beta_u P_u + \zeta_{uv}P_v$ and $\mathcal{P} = p_pP_p^2 + p_sP_s^2 + p_{ps}P_pP_s$.

Irrespective of input power levels and waveguide parameters, the solution (32) maximizes the functional F, and thus the net gain experienced by the signal during Raman amplification (for proof, see [91]). Hence, the optimal EMA axial profile of the SOI waveguide can be found by solving the system of four coupled nonlinear differential equations, which are given in (25) and (31), assuming that $A_{\rm eff}$ is given by (32). The four boundary conditions needed for solving these four equations come from the condition $\varphi(L) = 0$ and the three initial conditions:

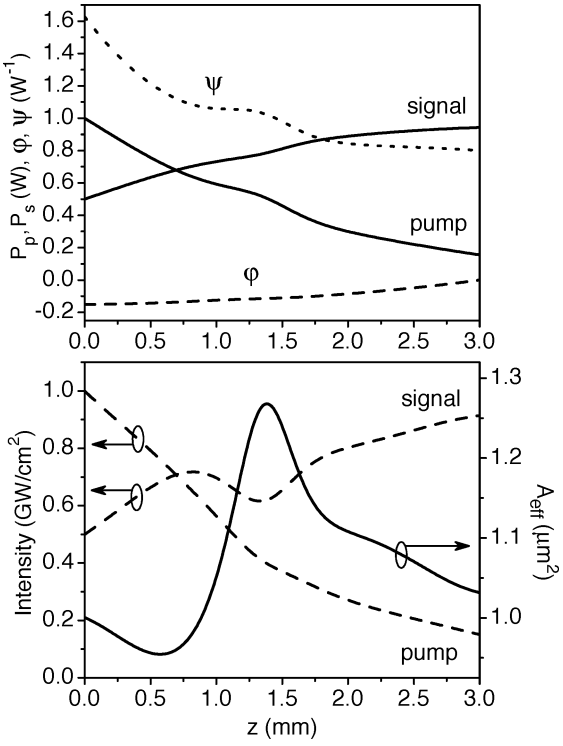

Fig. 5. (Upper panel) Solution of (25) and (31) for a 3-mm-long waveguide with input values $P_{p0} = 1$ W, $P_{s0} = 0.5$ W, and $A_0 = 1\,\mu\mathrm{m}^2$. Solid curves show the pump and signal powers; dashed and dotted curves represent the two auxiliary functions. (Lower panel) Optimized EMA profile (solid curve) and the pump and signal intensities (dashed curves) under the same conditions. Parameter values used are $\lambda_p = 1550$ nm, $\lambda_s = 1686$ nm, $\alpha_p = \alpha_s = 1$ dB/cm, $\beta_p = \beta_s = \beta_{ps} = 0.5$ cm/GW, and $\tau_c = 1$ ns (after [91]).

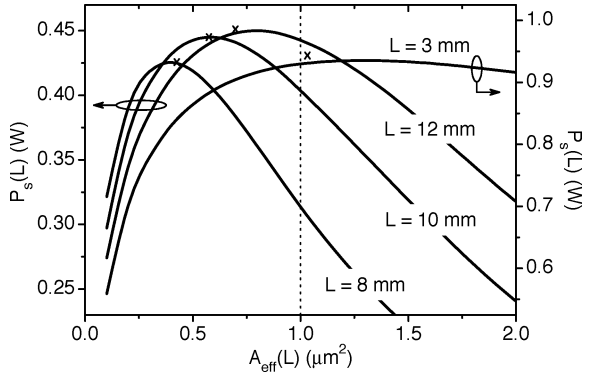

Fig. 6. Output signal power as a function of output EMA for linearly tapered waveguides of four different lengths when input pump power is 1 W and initial EMA is 1 $\mu\mathrm{m}^2$. Input signal power is 0.01 W for $L = 8$, 10, and 12 mm and 0.5 W for $L = 3$ mm. The central dotted line represents a waveguide with constant EMA. The crosses show signal powers and EMAs for EMA-optimized waveguides for the same input powers. Other parameter values are the same as in Fig. 5 (after [91]).

$P_p(0) = P_{p0}$, $P_s(0) = P_{s0}$, and $A_{\mathrm{eff}}(0) = A_0$. The last condition can also be used at $z = L$ if the objective is to design a Raman amplifier with a preset EMA at the output end of the amplifier.

C. Numerical Example

As an example, Fig. 5 shows the optimized solution in the case of a 3-mm-long amplifier. The upper panel represents variations of the pump and signal powers, as well as of the two auxiliary functions, along the amplifier length. The lower panel shows the optimum EMA profile (solid curve) together with the pump and signal intensities (dashed curves). The incident powers $P_{p0} = 1$ W and $P_{s0} = 0.5$ W are so high in this case that the optimum EMA increases by about 30% between 0.6 and 1.4 mm so that the pump and signal intensities decrease for a while to reduce the extent of pump depletion and to conserve pump's power for subsequent energy conversion closer to the waveguide output. Note that, even in this highly saturated regime, the pump is able to transfer about 85% of its power to the signal in spite of losses resulting from TPA and FCA.

To emphasize the role of waveguide tapering, Fig. 6 compares Raman amplification in optimized silicon waveguides with that occurring in untapered as well as linearly tapered waveguides. Solid curves show the dependance of output signal power on the output EMA for linearly tapered waveguides of four different lengths. The crosses represent the corresponding output signal powers realized with the optimum tapering. As one may expect, a silicon waveguide with a constant EMA all along its length performs the worst in some cases. For example, the output signal power is enhanced by a factor of nearly 3 for an 8-mm-long amplifier with the optimum EMA profile. A smaller enhancement (around 10%) occurs for a 10-mm-long waveguide, and nearly no enhancement is found for 3- and 12-mm-long waveguides. From a practical perspective, it is significant that, for each optimized amplifier, there exist a linearly tapered waveguide (its parameters are determined by the maxima of the solid curves) that gives nearly the same signal amplification. Thus, for example, instead of reproducing the modal area profile shown in the lower panel of Fig. 5, one can attain the same signal gain by fabricating a linearly tapered amplifier with an output EMA approximately equal to $1.3\ \mu\mathrm{m}^2$.

VII. Conclusion

For an intuitive understanding of nonlinear optical phenomena in silicon waveguides, numerical simulations should be supported by simple analytical solutions capable of providing a reasonable estimate of the physical quantity involved. Such solutions provide not only a rapid way of checking simulation results but also considerable physical insight that is often lost in voluminous data generated by numerical simulations. In this paper, we have discussed several analytical and semianalytical tools that have proved to be very successful in providing well-needed physical insight into the nonlinear effects. In many instances, the nontrivial information conveyed by the expressions resulting from the analytic methods cannot be easily extracted directly from pure numerical simulations.

Our first example considered propagation of short optical pulse and analyzed the impact of TPA, FCA, and FCD on SPM-induced spectral broadening. We then focused on Raman amplification in SOI waveguides when both the pump and the signal are in the form of CW waves. With a careful analysis of the approximate expressions describing the evolution of pump and signal intensities in a CW silicon Raman amplifier, we

theoretically predicted the possibility that RIN transfer from the pump to the signal can be avoided under some conditions. Such a prediction would not have been possible through a mere numerical analysis [88]. Another example is the prediction of the optimal longitudinal EMA profile of a silicon Raman amplifier that provides the highest net gain for a given pump power. Due to the presence of an infinite number of candidate profiles, it is almost impossible to predict the correct longitudinal mode area profile numerically. However, by a clever application of a standard variational technique, stemming originally from classical mechanics, we could derive a set of equations that can systematically generate the optimal EMA profile. Thereafter, a simple numerical solution of these equations provided us with an optimal amplifier design.

In conclusion, we would like to emphasize an important point. Even though the presence of many intricate nonlinearities makes the analysis of active and passive silicon waveguides quite a complex task, we have shown that modern mathematics and modern physics can be beautifully married with each other to generate very useful approximations. We believe that these methods are not only of methodological and heuristic interest but eventually pave the way for a better design optimization process.

REFERENCES

[1] G. W. Rieger, K. S. Virk, and J. F. Yong, "Nonlinear propagation of ultrafast 1.5 μm pulses in high-index-contrast silicon-on-insulator waveguides," *Appl. Phys. Lett.*, vol. 84, pp. 900–902, 2004.

[2] A. R. Cowan, G. W. Rieger, and J. F. Young, "Nonlinear transmission of 1.5 μm pulses through single-mode silicon-on-insulator waveguide structures," *Opt. Exp.*, vol. 12, pp. 1611–1621, 2004.

[3] R. Claps, D. Dimitropoulos, V. Raghunathan, Y. Han, and B. Jalali, "Observation of stimulated Raman scattering in silicon waveguides," *Opt. Exp.*, vol. 11, pp. 1731–1739, 2003.

[4] E. Dulkeith, F. Xia, L. Schares, W. M. J. Green, and Y. A. Vlasov, "Group index and group velocity dispersion in silicon on insulator photonic wires," *Opt. Exp.*, vol. 14, pp. 3853–3863, 2006.

[5] A. C. Turner, C. Manolatou, B. S. Schmidt, M. Lipson, M. A. Foster, J. E. Sharping, and A. L. Gaeta, "Tailored anomalous GVD in Si channel waveguides," *Opt. Exp.*, vol. 14, pp. 4357–4362, 2006.

[6] J. Zhang, Q. Lin, G. Piredd, R. W. Boyd, G. P. Agrawal, and P. M. Fauchet, "Optical solitons in a silicon waveguide," *Opt. Exp.*, vol. 15, pp. 7682–7688, 2007.

[7] I.-W. Hsieh, X. Chen, J. I. Dadap, N. C. Panoiu, and R. M. Osgood, Jr., "Cross-phase modulation-induced spectral and temporal effects on co-propagating femtosecond pulses in silicon photonic wires," *Opt. Exp.*, vol. 15, pp. 1135–1146, 2007.

[8] D. Dimitripoulos, R. Jhavery, R. Claps, J. C. S. Woo, and B. Jalali, "Lifetime of photogenerated carriers in silicon-on-insulator rib waveguides," *Appl. Phys. Lett.*, vol. 86, pp. 071115-1–071115-3, 2005.

[9] T. K. Liang and H. K. Tsang, "Nonlinear absorption and Raman scattering in silicon-on-insulator optical waveguides," *IEEE J. Sel. Topics Quantum Electron.*, vol. 10, no. 5, pp. 1149–1153, Sep./Oct. 2004.

[10] I.-W. Hsieh, X. Chen, J. I. Dadap, N. C. Panoiu, R. M. Osgood, Jr., S. J. McNab, and Y. A. Vlasov, "Ultrafast-pulse self-phase modulation and third-order dispersion in Si photonic wire-waveguides," *Opt. Exp.*, vol. 14, pp. 12380–12387, 2006.

[11] W. Ding, C. Benton, A. V. Gorbach, W. J. Wadsworth, J. C. Knight, D. V. Skryabin, M. Gnan, M. Sorrel, and R. M. De La Rue, "Solitons and spectral broadening in long silicon-on-insulator photonic wires," *Opt. Exp.*, vol. 16, pp. 3310–3319, 2008.

[12] Q. Lin, O. J. Painter, and G. P. Agrawal, "Nonlinear optical phenomena in silicon waveguides: Modelling and applications," *Opt. Exp.*, vol. 15, pp. 16604–16644, 2007.

[13] X. Chen, N. C. Panoiu, and R. M. Osgood, "Theory of Raman-mediated pulsed amplification in silicon-wire waveguides," *IEEE J. Quantum Electron.*, vol. 42, no. 2, pp. 160–170, Feb. 2006.

[14] D. Dimitropoulos, B. Houshmand, R. Claps, and B. Jalali, "Coupled-mode theory of Raman effect in silicon-on-insulator waveguides," *Opt. Lett.*, vol. 28, pp. 1954–1956, 2003.

[15] X. Chen, N. Panoiu, I. Hsieh, J. I. Dadap, and R. M. Osgood, Jr., "Third-order dispersion and ultrafast pulse propagation in silicon wire waveguides," *IEEE Photon. Technol. Lett.*, vol. 18, no. 24, pp. 2617–2619, Dec. 2006.

[16] L. Yin, Q. Lin, and G. P. Agrawal, "Dispersion tailoring and soliton propagation in silicon waveguides," *Opt. Lett.*, vol. 31, pp. 1295–1297, 2006.

[17] V. M. N. Passaro and F. D. Leonardis, "Space-time modeling of Raman pulses in silicon-on-insulator optical waveguides," *J. Lightw. Technol.*, vol. 24, no. 7, pp. 2920–2931, Jul. 2006.

[18] V. M. N. Passaro and F. D. Leonardis, "Solitons in SOI optical waveguides," *Adv. Stud. Theor. Phys.*, vol. 2, pp. 769–785, 2008.

[19] J. I. Dadap, N. C. Panoiu, X. Chen, I. W. Hsieh, X. Liu, C. Y. Chou, E. Dulkeith, S. J. McNab, F. Xia, W. M. J. Green, L. Sekaric, Y. A. Vlasov, and R. M. Osgood, Jr., "Nonlinear-optical phase modification in dispersion-engineered Si photonic wires," *Opt. Exp.*, vol. 16, pp. 1280–1299, 2008.

[20] M. Krause, H. Renner, S. Fathpour, B. Jalali, and E. Brinkmeyer, "Gain enhancement in cladding-pumped silicon Raman amplifiers," *IEEE J. Quantum Electron.*, vol. 44, no. 7, pp. 692–704, Jul. 2008.

[21] V. S. Avshar and T. M. Monro, "A full vectorial model for pulse propagation in emerging waveguides with subwavelength structures part I: Kerr nonlinearity," *Opt. Exp.*, vol. 17, pp. 2298–2318, 2009.

[22] R. M. Osgood, Jr., N. C. Panoiu, J. I. Dadap, X. Liu, X. Chen, I. W. Hsieh, E. Dulkeith, W. M. J. Green, and Y. A. Vlasov, "Engineering nonlinearities in nanoscale optical systems: Physics and applications in dispersion-engineered silicon nanophotonic wires," *Adv. Opt. Photon.*, vol. 1, pp. 162–235, 2009.

[23] R. A. Soref, "The past, present, and future of silicon photonics," *IEEE J. Sel. Topics Quantum Electron.*, vol. 12, no. 6, pp. 1678–1687, Nov./Dec. 2006.

[24] G. T. Reed and A. P. Knights, *Silicon Photonics: An Introduction*. Hoboken, NJ: Wiley, 2004.

[25] B. Jalali, O. Boyraz, V. Raghunathan, D. Dimitropoulos, and P. Koonath, "Silicon Raman amplifiers, lasers and their applications," in *Proc. SPIE, Active Passive Opt. Compon. WDM Commun. V*, A. K. Dutta, Y. Ohishi, N. K. Dutta, and J. Moerk, Eds., 2005, vol. 6014, pp. 21–26.

[26] B. Jalali, V. Raghunathan, D. Dimitropoulos, and O. Boyraz, "Raman-based silicon photonics," *IEEE J. Sel. Topics Quantum Electron.*, vol. 12, no. 3, pp. 412–421, May/Jun. 2006.

[27] C. Koos, L. Jacome, C. Poulton, J. Leuthold, and W. Freude, "Nonlinear silicon-on-insulator waveguides for all-optical processing," *Opt. Exp.*, vol. 15, pp. 5976–5990, 2007.

[28] M. A. Foster, A. C. Turner, M. Lipson, and A. L. Gaeta, "Nonlinear optics in photonic nanowires," *Opt. Exp.*, vol. 16, pp. 1300–1320, 2008.

[29] O. Boyraz, P. Koonath, V. Raghunathan, and B. Jalali, "All optical switching and continuum generation in silicon waveguides," *Opt. Exp.*, vol. 12, pp. 4094–4102, 2004.

[30] B. Jalali, S. Yegnanarayanan, T. Yoon, T. Yoshimoto, I. Rendina, and F. Coppinger, "Advances in silicon-on-insulator optoelectronics," *IEEE J. Sel. Topics Quantum Electron.*, vol. 4, no. 6, pp. 938–947, Nov./Dec. 1998.

[31] H. K. Tsang and Y. Liu, "Nonlinear optical properties of silicon waveguides," *Semicond. Sci. Technol.*, vol. 23, pp. 064007-1–064007-9, 2008.

[32] R. S. Jacobsen, K. N. Andersen, P. I. Borel, J. Fage-Pedersen, L. H. Frandsen, O. Hansen, M. Kristensen, A. V. Lavrinenko, G. Moulin, H. Ou, C. Peucheret, B. Zsigri, and A. Bjarklev, "Strained silicon as a new electro-optic material," *Nature*, vol. 441, pp. 199–202, 2006.

[33] M. Dinu, F. Quochi, and H. Garcia, "Third-order nonlinearities in silicon at telecom wavelengths," *Appl. Phys. Lett.*, vol. 82, pp. 2954–2956, 2003.

[34] R. Claps, D. Dimitropoulos, and B. Jalali, "Stimulated Raman scattering in silicon waveguides," *Electron. Lett.*, vol. 38, pp. 1352–1354, 2002.

[35] R. Claps, D. Dimitropoulos, V. Raghunathan, Y. Han, and B. Jalali, "Observation of stimulated Raman amplification in silicon waveguides," *Opt. Exp.*, vol. 11, pp. 1731–1739, 2003.

[36] T. K. Liang and H. K. Tsang, "Role of free carriers from two-photon absorption in Raman amplification in silicon-on-insulator waveguides," *Appl. Phys. Lett.*, vol. 84, pp. 2745–2747, 2004.

[37] R. Claps, V. Raghunathan, D. Dimitropoulos, and B. Jalali, "Influence of nonlinear absorption on Raman amplification in silicon-on-insulator waveguides," *Opt. Exp.*, vol. 12, pp. 2774–2780, 2004.

[38] O. Boyraz and B. Jalali, "Demonstration of 11 dB fiber-to-fiber gain in a silicon Raman amplifier," *IEICE Electron. Exp.*, vol. 1, pp. 429–434, 2004.

[39] A. Liu, H. Rong, M. Paniccia, O. Cohen, and D. Hak, "Net optical gain in a low loss silicon-on-insulator waveguide by stimulated Raman scattering," *Opt. Exp.*, vol. 12, pp. 4261–4268, 2004.

[40] R. Espinola, J. Dadap, R. Osgood, S. J. McNab, and Y. A. Vlasov, "Raman amplification in ultrasmall silicon-on-insulator wire waveguides," *Opt. Exp.*, vol. 12, pp. 3713–3718, 2004.

[41] R. Jones, H. Rong, A. Liu, A. W. Fang, M. J. Paniccia, D. Hak, and O. Cohen, "Net continuous-wave optical gain in a low loss silicon-on-insulator waveguide by stimulated Raman scattering," *Opt. Exp.*, vol. 13, pp. 519–525, 2005.

[42] S. Fathpour, K. K. Tsia, and B. Jalali, "Energy harvesting in silicon Raman amplifiers," *Appl. Phys. Lett.*, vol. 89, pp. 061109-1–061109-3, 2006.

[43] R. Jones, A. Liu, H. Rong, M. Paniccia, O. Cohen, and D. Hak, "Lossless optical modulation in a silicon waveguide using stimulated Raman scattering," *Opt. Exp.*, vol. 13, pp. 1716–1723, 2005.

[44] R. Claps, D. Dimitropoulos, Y. Han, and B. Jalali, "Observation of Raman emission in silicon waveguides at 1.54 μm," *Opt. Exp.*, vol. 10, pp. 1305–1313, 2002.

[45] O. Boyraz and B. Jalali, "Demonstration of a silicon Raman laser," *Opt. Exp.*, vol. 12, pp. 5269–5273, 2004.

[46] M. Krause, H. Renner, and E. Brinkmeyer, "Analysis of Raman lasing characteristics in silicon-on-insulator waveguides," *Opt. Exp.*, vol. 12, pp. 5703–5710, 2004.

[47] H. Renner, M. Krause, and E. Brinkmeyer, "Maximal gain and optimal taper design for Raman amplifiers in silicon-on-insulator waveguides," presented at the Integr. Photon. Res. Appl. Top. Meeting (IPRA 2005), San Diego, CA, Paper JWA3..

[48] M. Krause, H. Renner, and E. Brinkmeyer, "Efficiency increase of silicon-on-insulator Raman lasers by reduction of free-carrier absorption in tapered waveguides," in *Proc. Conf. Lasers Electr.-Opt. (CLEO 2005)*, May, vol. 2, pp. 1548–1550, Paper CThB1.

[49] H. Rong, A. Liu, R. Jones, O. Cohen, D. Hak, R. Nicolaescu, A. Fang, and M. Paniccia, "An all-silicon Raman laser," *Nature*, vol. 433, pp. 292–294, 2005.

[50] O. Boyraz and B. Jalali, "Demonstration of directly modulated silicon Raman laser," *Opt. Exp.*, vol. 13, pp. 796–800, 2005.

[51] H. Rong, R. Jones, A. Liu, O. Cohen, D. Hak, A. Fang, and M. Pannicia, "A continuous-wave Raman silicon laser," *Nature*, vol. 433, pp. 725–728, 2005.

[52] M. Krause, H. Renner, and E. Brinkmeyer, "Efficient Raman lasing in tapered silicon waveguides," *Spectroscopy*, vol. 21, no. 1, pp. 26–32, 2006.

[53] R. Dekker, A. Driessen, T. Wahlbrink, C. Moormann, J. Niehusmann, and M. Först, "Ultrafast Kerr-induced all-optical wavelength conversion in silicon waveguides using 1.55 μm femtosecond pulses," *Opt. Exp.*, vol. 14, pp. 8336–8346, 2006.

[54] E. Dulkeith, Y. A. Vlasov, X. Chen, N. C. Panoiu, and R. M. Osgood, Jr., "Self-phase-modulation in submicron silicon-on-insulator photonic wires," *Opt. Exp.*, vol. 14, pp. 5524–5534, 2006.

[55] L. Yin, Q. Lin, and G. P. Agrawal, "Soliton fission and supercontinuum generation in silicon waveguides," *Opt. Lett.*, vol. 32, pp. 391–393, 2007.

[56] O. Boyraz, T. Indukuri, and B. Jalali, "Self-phase-modulation induced spectral broadening in silicon waveguides," *Opt. Exp.*, vol. 12, pp. 829–834, 2004.

[57] I.-W. Hsieh, X. Chen, X. Liu, J. I. Dadap, N. C. Panoiu, C. Y. Chou, F. Xia, W. M. Green, Y. A. Vlasov, and R. M. Osgood, Jr., "Supercontinuum generation in silicon photonic wires," *Opt. Exp.*, vol. 15, pp. 15242–15249, 2007.

[58] R. Claps, V. Raghunathan, D. Dimitropoulos, and B. Jalali, "Anti-Stokes Raman conversion in silicon waveguides," *Opt. Exp.*, vol. 11, pp. 2862–2872, 2003.

[59] D. Dimitropoulos, V. Raghunathan, R. Claps, and B. Jalali, "Phase-matching and nonlinear optical processes in silicon waveguides," *Opt. Exp.*, vol. 12, pp. 149–160, 2004.

[60] V. Raghunathan, R. Claps, D. Dimitropoulos, and B. Jalali, "Parametric Raman wavelength conversion in scaled silicon waveguides," *J. Lightw. Technol.*, vol. 23, no. 6, pp. 2094–2012, Jun. 2005.

[61] R. L. Espinola, J. I. Dadap, R. M. Osgood, S. J. McNab, and Y. A. Vlasov, "C-band wavelength conversion in silicon photonic wire waveguides," *Opt. Exp.*, vol. 13, pp. 4341–4349, 2005.

[62] H. Fukuda, K. Yamada, T. Shoji, M. Takahashi, T. Tsuchizawa, T. Watanabe, J. Takahashi, and S. Itabashi, "Four-wave mixing in silicon wire waveguides," *Opt. Exp.*, vol. 13, pp. 4629–4637, 2005.

[63] H. Rong, Y. H. Kuo, A. Liu, M. Paniccia, and O. Cohen, "High efficiency wavelength conversion of 10 Gb/s data in silicon waveguides," *Opt. Exp.*, vol. 14, pp. 1182–1188, 2006.

[64] Q. Lin, J. Zhang, P. M. Fauchet, and G. P. Agrawal, "Ultrabroadband parametric generation and wavelength conversion in silicon waveguides," *Opt. Exp.*, vol. 14, pp. 4786–4799, 2006.

[65] M. Krause, R. Draheim, H. Renner, and E. Brinkmeyer, "Cascaded silicon Raman lasers as mid-infrared sources," *Electron. Lett.*, vol. 42, pp. 2006–2031, 2006.

[66] M. A. Foster, R. Salem, D. F. Geraghty, A. C. Turner-Foster, M. Lipson, and A. L. Gaeta, "Silicon-chip-based ultrafast optical oscilloscope," *Nature*, vol. 456, pp. 81–85, 2008.

[67] T. Liang, L. Nunes, T. Sakamoto, K. Sasagawa, T. Kawanishi, M. Tsuchiya, G. Priem, D. V. Thourhout, P. Dumon, R. Baets, and H. Tsang, "Ultrafast all-optical switching by cross-absorption modulation in silicon wire waveguides," *Opt. Exp.*, vol. 13, pp. 7298–7303, 2005.

[68] T. K. Liang, L. R. Nunes, M. Tsuchiya, K. S. Abedin, T. Miyazaki, D. V. Thourhout, W. Bogaerts, P. Dumon, R. Baets, and H. Tsang, "High speed logic gate using two-photon absorption in silicon waveguides," *Opt. Commun.*, vol. 265, pp. 171–174, 2006.

[69] M. W. Geis, S. J. Spector, R. C. Williamson, and T. M. Lyszczarz, "Submicrosecond, submilliwatt, silicon-on-insulator thermooptic switch," *IEEE Photon. Technol. Lett.*, vol. 16, no. 11, pp. 2514–2516, Nov. 2004.

[70] H. K. Tsang, C. S. Wong, T. K. Liang, I. E. Day, S. W. Roberts, A. Harpin, J. Drake, and M. Asghari, "Optical dispersion, two-photon absorption, and self-phase modulation in silicon waveguides at 1.5 μm wavelength," *Appl. Phys. Lett.*, vol. 80, pp. 416–418, 2002.

[71] Y.-H. Kao, T. J. Xia, and M. N. Islam, "Limitations on ultrafast optical switching in a semiconductor laser amplifier operating at transparency current," *J. Appl. Phys.*, vol. 86, pp. 4740–4747, 1999.

[72] D. J. Moss, L. Fu, I. Littler, and B. J. Eggleton, "Ultrafast all-optical modulation via two-photon absorption in silicon-on-insulator waveguides," *Electron. Lett.*, vol. 41, no. 6, pp. 320–321, Mar. 2005.

[73] E. K. Tien, N. S. Yuksek, F. Qian, and O. Boyraz, "Pulse compression and modelocking by using TPA in silicon waveguides," *Opt. Exp.*, vol. 15, pp. 6500–6506, 2007.

[74] E. K. Tien, F. Qian, N. S. Yuksek, and O. Boyraz, "Influence of nonlinear loss competition on pulse compression and nonlinear optics in silicon," *Appl. Phys. Lett.*, vol. 91, pp. 201115-1–201115-3, 2007.

[75] T. K. Liang, H. K. Tsang, I. E. Day, J. Drake, A. P. Knights, and M. Asghari, "Silicon waveguide two-photon absorption detector at 1.5 μm wavelength for autocorrelation measurements," *Appl. Phys. Lett.*, vol. 81, pp. 1323–1325, 2002.

[76] D. T. Reid and W. Sibbett, "Commercial semiconductor devices for two photon absorption autocorrelation of ultrashort light pulses," *Appl. Opt.*, vol. 37, pp. 8142–8144, 1998.

[77] G. P. Agrawal, *Nonlinear Fiber Optics*. Boston, MA: Academic, 2007.

[78] N. Suzuki, "FDTD analysis of two-photon absorption and free-carrier absorption in Si high-index-contrast waveguides," *J. Lightw. Technol.*, vol. 25, no. 9, pp. 2495–2501, Sep. 2007.

[79] R. M. Joseph and A. Taflove, "FDTD Maxwell's equations models for nonlinear electrodynamics and optics," *IEEE Trans. Antennas Propag.*, vol. 45, no. 3, pp. 364–374, Mar. 1997.

[80] R. W. Ziolkowski, "The incorporation of microscopic material models into the FDTD approach for ultrafast optical pulse simulations," *IEEE Trans. Antennas Propag.*, vol. 45, no. 3, pp. 375–391, Mar. 1997.

[81] R. W. Boyd, *Nonlinear Optics*. Boston, MA: Academic, 2003.

[82] I. D. Rukhlenko, M. Premaratne, C. Dissanayake, and G. P. Agrawal, "Nonlinear pulse evolution in silicon waveguides: An approximate analytic approach," *J. Lightw. Technol.*, vol. 27, no. 15, pp. 3241–3248, Aug. 2009.

[83] C. Headley and G. P. Agrawal, Eds., *Raman Amplification in Fiber-Optic Communication Systems*. San Diego, CA: Academic, 2005.

[84] L. Yin and G. P. Agrawal, "Impact of two-photon absorption on self-phase modulation in silicon waveguides," *Opt. Lett.*, vol. 32, pp. 2031–2033, 2007.

[85] L. B. Fu, M. Rochette, V. G. Ta'eed, D. J. Moss, and B. J. Eggleton, "Investigation of self-phase modulation based optical regeneration in single mode As_2Se_3 chalcogenide glass fiber," *Opt. Exp.*, vol. 13, pp. 7637–7644, 2005.

[86] I. D. Rukhlenko, M. Premaratne, C. Dissanayake, and G. P. Agrawal, "Continuous-wave Raman amplification in silicon waveguides: Beyond

the undepleted pump approximation," *Opt. Lett.*, vol. 34, pp. 536–538, 2009.
[87] A. D. Polyanin and V. F. Zaitsev, *Handbook of Exact Solutions for Ordinary Differential Equations*. London, U.K./Boca Raton, FL: Chapman & Hall/CRC Press, 2003.
[88] X. Sang, D. Dimitropoulos, B. Jalali, and O. Boyraz, "Influence of pump-to-signal RIN transfer on noise figure in silicon Raman amplifiers," *IEEE Photon. Technol. Lett.*, vol. 20, no. 24, pp. 2021–2023, Dec. 2008.
[89] C. R. S. Fludger, V. Handerek, and R. J. Mears, "Pump to signal RIN transfer in Raman fiber amplifiers," *J. Lightw. Technol.*, vol. 19, no. 8, pp. 1140–1148, Aug. 2001.
[90] S. Roy, S. K. Bhadra, and G. P. Agrawal, "Raman amplification of optical pulses in silicon waveguides: Effects of finite gain bandwidth, pulse width, and chirp," *J. Opt. Soc. Amer. B*, vol. 26, pp. 17–25, 2009.
[91] I. D. Rukhlenko, M. Premaratne, C. Dissanayake, and G. P. Agrawal, "Maximization of net optical gain in silicon-waveguide Raman amplifiers," *Opt. Exp.*, vol. 17, pp. 5807–5814, 2009.
[92] C. Fox, *An Introduction to the Calculus of Variations*. New York: Dover, 1987.

Ivan D. Rukhlenko received the B.Sc. and M.Sc. degrees in physics (with honors) from St. Petersburg State Technical University, St. Petersburg, Russia, in 2001 and 2003, respectively, and the Ph.D. degree in optics from St. Petersburg State University of Informational Technologies, Mechanics and Optics, St. Petersburg, in 2006.

From 2006 to 2008, he was a Research Fellow with the Department Optics of Nanostructures, Center of Informational Optical Technologies, St. Petersburg State University of Informational Technologies, Mechanics and Optics. He is currently a Research Fellow with the Advanced Computing and Simulation Laboratory (AχL), Department of Electrical and Computer Systems Engineering, Monash University, Clayton, Vic., Australia. He has authored or coauthored more than ten research papers in the area of physics of low-dimensional structures. His current research interests include nonlinear effects in silicon photonics, dynamics of spectroscopic transitions in quantum dots, and quantum dot secondary emission and propagation of elementary excitations in semiconductor heterostructures.

Malin Premaratne (S'95–M'98–SM'03) received the B.Sc. degree in mathematics, the B.E. degree in electrical and electronics engineering (with first-class honors), and the Ph.D. degree from the University of Melbourne, Melbourne, Victoria, Australia, in 1995, 1995, and 1998, respectively.

From 1998 to 2000, he was with the Photonics Research Laboratory, a division of the Australian Photonics Cooperative Research Center (APCRC), University of Melbourne, where he was the Coproject Leader of the APCRC Optical Amplifier Project, and was also associated with Telstra, Australia, and Hewlett Packard, USA. From 2000 to 2003, he was involved with several leading start-ups in the photonic area either as an Employee or a Consultant, and has also been a member of the Editorial Boards of the International Society for Optical Engineers (SPIE)/Kluwer and Wiley publishers in the optical communications area. From 2001 to 2003, he was the Product Manger (Research and Development) of VPI Systems Optical Systems Group. Since 2003, he guided the research program in high-performance computing applications to complex systems simulations at the Advanced Computing and Simulation Laboratory (AχL), Monash University, Clayton, Vic., Australia, where he is currently the Research Director and an Associate Professor. He has authored or coauthored more than 100 research papers in the areas of semiconductor lasers, erbium-doped fiber amplifier and Raman amplifiers, optical network design algorithms, and numerical simulation techniques. He is also a Visiting Researcher with the University of Melbourne, Australian National University, Canberra, A.C.T., Australia, the University of California–Los Angeles (UCLA), Los Angeles, and the University of Rochester, Rochester, NY.

Dr. Premaratne is a Fellow of the Institution of Engineers Australia (FIEAust). He is an executive member of the IEAust, Victoria Division, Australia. Since 2001, he has been the Chairman of the IEEE Lasers and Electro-Optics Society in Victoria, Australia.

Govind P. Agrawal (M'83–SM'86–F'96) received the B.Sc. degree from the University of Lucknow, Lucknow, India, in 1969, and the M.Sc. and Ph.D. degrees from the Indian Institute of Technology Delhi, New Delhi, India, in 1971 and 1974, respectively.

He was with the Ecole Polytechnique, France, the City University of New York, New York, and AT&T Bell Laboratories, Murray Hill, NJ. In 1989, he joined the faculty of the Institute of Optics, University of Rochester, Rochester, NY, where he is currently a Professor of optics. His current research interests include optical communications, nonlinear optics, and laser physics. He is the author or coauthor of more than 300 research papers, several book chapters and review articles, and seven books including *Semiconductor Laser* (Norwell, MA: Kluwer, 2nd ed., 1993), *Fiber-Optic Communication Systems* (Hoboken, NJ: Wiley, 3rd ed., 2002), *Nonlinear Fiber Optics* (Boston, MA: Academic, 4th ed., 2007), *Applications of Nonlinear Fiber Optics* (Boston, MA: Academic, 2nd ed., 2008), *Optical Solitons: From Fibers to Photonic Crystals* (San Diego, CA: Academic, 2003), *Lightwave Technology: Components and Devices* (Hoboken, NJ: Wiley, 2004), and *Lightwave Technology: Telecommunication System* (Hoboken, NJ: Wiley, 2005).

Prof. Agrawal is a Fellow of the Optical society of America (OSA). He is also a Life Fellow of the Optical Society of India. He has participated multiple times in organizing technical conferences sponsored by the IEEE and the OSA. He was the General Cochair of the Quantum Electronics and Laser Science Conference in 2001. He was a member of the Program Committee of the Conference on Lasers and Electro-Optics in 2004 and 2005.